Atmos. Chem. Phys. Discuss., 6, 9765–9821, 2006
www.atmos-chem-phys-discuss.net/6/9765/2006/

Atmospheric Chemistry and Physics Discussions

Validation of MIPAS $ClONO_2$ measurements

M. Höpfner[1], T. von Clarmann[1], H. Fischer[1], B. Funke[2], N. Glatthor[1], U. Grabowski[1], S. Kellmann[1], M. Kiefer[1], A. Linden[1], M. Milz[1], T. Steck[1], G. P. Stiller[1], P. Bernath[3], C. E. Blom[1], Th. Blumenstock[1], C. Boone[3], K. Chance[4], M. T. Coffey[5], F. Friedl-Vallon[1], D. Griffith[6], J. W. Hannigan[5], F. Hase[1], N. Jones[6], K. W. Jucks[7], C. Keim[1], A. Kleinert[1], W. Kouker[1], G. Y. Liu[1], E. Mahieu[8], J. Mellqvist[9], S. Mikuteit[1], J. Notholt[10], H. Oelhaf[1], C. Piesch[1], T. Reddmann[1], R. Ruhnke[1], M. Schneider[1], A. Strandberg[9], G. Toon[11], K. A. Walker[3], T. Warneke[10], G. Wetzel[1], S. Wood[12], and R. Zander[8]

[1]Institut für Meteorologie und Klimaforschung, Forschungszentrum Karlsruhe, Germany
[2]Instituto de Astrofísica de Andalucía, Granada, Spain
[3]Department of Chemistry, University of Waterloo, Ontario, Canada
[4]Harvard-Smithsonian Center for Astrophysics, Atomic and Molecular Physics Division, Cambridge, MA, USA
[5]Atmospheric Chemistry Division, National Center for Atmospheric Research, Boulder, CO, USA
[6]Department of Chemistry, University of Wollongong, Australia

[7] Harvard-Smithsonian Center for Astrophysics, Optical and Infrared Astronomy Division, Cambridge, MA, USA
[8] Institut d'Astrophysique et de Géophysique, Université de Liège, Belgium
[9] Department of Radio and Space Science, Chalmers University of Technology, Göteborg, Sweden
[10] Institut für Umweltphysik, Universität Bremen, Germany
[11] Jet Propulsion Laboratory, California Institute of Technology, Pasadena, CA, USA
[12] National Institute of Water and Atmospheric Research, Lauder, New-Zealand

Received: 8 August 2006 – Accepted: 15 September 2006 – Published: 5 October 2006

Correspondence to: M. Höpfner (michael.hoepfner@imk.fzk.de)

Abstract

Altitude profiles of $ClONO_2$ retrieved with the IMK (Institut für Meteorologie und Klimaforschung) science-oriented data processor from MIPAS/Envisat (Michelson Interferometer for Passive Atmospheric Sounding on Envisat) mid-infrared limb emission measurements between July 2002 and March 2004 have been validated by comparison with balloon-borne (Mark IV, FIRS2, MIPAS-B), airborne (MIPAS-STR), ground-based (Spitsbergen, Thule, Kiruna, Harestua, Jungfraujoch, Izaña, Wollongong, Lauder), and spaceborne (ACE-FTS) observations. With few exceptions we found very good agreement between these instruments and MIPAS with no evidence for any bias in most cases and altitude regions. For balloon-borne measurements typical absolute mean differences are below 0.05 ppbv over the whole altitude range from 10 to 39 km. In case of ACE-FTS observations mean differences are below 0.03 ppbv for observations below 26 km. Above this altitude the comparison with ACE-FTS is affected by the photochemically induced diurnal variation of $ClONO_2$. Correction for this by use of a chemical transport model led to an overcompensation of the photochemical effect by up to 0.1 ppbv at altitudes of 30–35 km in case of MIPAS-ACE-FTS comparisons while for the balloon-borne observations no such inconsistency has been detected. The comparison of MIPAS derived total column amounts with ground-based observations revealed no significant bias in the MIPAS data. Mean differences between MIPAS and FTIR column abundances are $0.11\pm0.12\times10^{14}$ cm^{-2} (1.0±1.1%) and $-0.09\pm0.19\times10^{14}$ cm^{-2} (−0.8±1.7%), depending on the coincidence criterion applied. χ^2 tests have been performed to assess the combined precision estimates of MIPAS and the related instruments. When no exact coincidences were available as in case of MIPAS – FTIR or MIPAS – ACE-FTS comparisons it has been necessary to take into consideration a coincidence error term to account for χ^2 deviations. From the resulting χ^2 profiles there is no evidence for a systematic over/underestimation of the MIPAS random error analysis.

1 Introduction

Chlorine nitrate ($ClONO_2$) is a major temporary reservoir gas of chlorine in the stratosphere. It plays an important role in the processes of ozone depletion (Solomon, 1999). Though $ClONO_2$ has recently been observed by in-situ methods (Stimpfle et al., 1999; Marcy et al., 2005), by far most measurements have been made remotely by analysis of its rovibrational bands in the mid-infrared atmospheric window through high-resolution spectroscopy.

Stratospheric $ClONO_2$ was first detected by solar absorption spectroscopy from balloons (Murcray et al., 1979; Rinsland et al., 1985) and from space (Zander et al., 1986) by the Atmospheric Trace Molecule Spectroscopy (ATMOS) instrument. ATMOS also provided spaceborne measurements of $ClONO_2$ profiles in March 1992, April 1993 and November 1994 (Rinsland et al., 1994, 1995, 1996; Zander et al., 1996). Column amounts from ground-based solar absorption observations have been first reported by Zander and Demoulin (1988) over the Jungfraujoch and by Farmer et al. (1987) over McMurdo.

Early sun-independent determination of $ClONO_2$ through mid-IR thermal emission spectroscopy are balloon-borne measurements by the Michelson Interferometer for Passive Atmospheric Sounding (MIPAS-B) (von Clarmann et al., 1993; Oelhaf et al., 1994), airborne observation by MIPAS-FT (Blom et al., 1995), and spaceborne data by the Cryogenic Limb Array Etalon Spectrometer (CLAES) (Roche et al., 1993, 1994). CLAES obtained nearly global fields of $ClONO_2$ from 25 October 1991 until 5 May 1993 which have been validated by Mergenthaler et al. (1996).

In this paper we report on the validation of atmospheric $ClONO_2$ profiles derived from MIPAS observations made on board the polar orbiting satellite Envisat between mid-2002 and end of March 2004.

2 MIPAS $ClONO_2$ data analysis

MIPAS is a Fourier transform spectrometer sounding the thermal emission of the earth's atmosphere between 685 and 2410 cm^{-1} (14.6–4.15 μm) in limb geometry. The maximum optical path difference (OPD) of MIPAS is 20 cm. For the present data analysis the spectra have been apodised with the Norton-Beer strong function (Norton and Beer, 1976) resulting in an apodised spectral resolution (FWHM) of 0.048 cm^{-1}. The field-of-view of the instrument at the tangent points is about 3 km in the vertical and 30 km in the horizontal. In the standard observation mode in one limb-scan 17 tangent points are observed with nominal altitudes 6, 9, 12,..., 39, 42, 47, 52, 60, and 68 km. In this mode about 73 limb scans are recorded per orbit with 14.3 orbits per day. The measurements of each orbit cover nearly the complete latitude range from about 87° S to 89° N. In the described standard mode MIPAS measured quasi-continuously from July 2002 until end of March 2004 when operation was stopped for investigation of instabilities of the interferometer drive velocity. Measurements have been resumed in early 2005, however, with poorer spectral resolution and finer tangent altitude grid.

Here we concentrate on the validation of $ClONO_2$ profiles derived from the first measurement period. $ClONO_2$ is one of the trace-gases retrieved at the Institut für Meteorologie und Klimaforschung, Forschungszentrum Karlsruhe (IMK) as an off-line product and is available at http://www-imk.fzk.de/asf/ame/envisat-data/. $ClONO_2$ is not included in the operational level 2 data analysis under ESA responsibility. The present validation work is performed with IMK data versions V3O_CLONO2_10 and V3O_CLONO2_11 which are consistent. These retrievals are based on reprocessed ESA level 1b products (calibrated spectra) Version 4.61 and 4.62.

The data processing chain for $ClONO_2$ has been described in detail by Höpfner et al. (2004). The IMK version of the data discussed there was V1_CLONO2_1 which differs from the version V3O_CLONO2_10/11 in several aspects: (1) near-real-time ESA level 1b data version 4.53 was used then, (2) latitude-band dependent a-priori profiles were assumed while for V3O_CLONO2_10/11 flat zero a-priori profiles are used, and

(3) the height-dependent regularization strength has been changed to allow for more sensitivity at lower and higher altitudes.

For characterisation of the altitude resolution of a typical $ClONO_2$ profile of the data version used in this paper, Fig. 1 shows as an example the averaging kernel matrix **A** of a mid-latitude MIPAS measurement. This observation is validated against a MIPAS-B observation below in Sect. 3.1.1. The rows of **A** represent the contributions of the real profile to the retrieved profile whereas the columns are the response of the retrieval scheme to a delta function in the related altitude (Rodgers, 2000). The full width at half maximum of the columns of **A** can be used as a measure for the vertical resolution which ranges from 3.2 to 8.5 km in the altitude region 8 to 40 km for our $ClONO_2$ retrievals.

The linear error analysis of the previous example from mid-latitudes is given in Table 1. It shows that the main error sources are the spectral noise of the instrument and the uncertainty of spectroscopic data. This is consistent with the error estimation of a polar profile discussed in Höpfner et al. (2004). For the comparisons with other measurements we use the total estimated random error which we define as the total error given in Table 1 without the error due non-local thermodynamic equilibrium (non-LTE), which is anyway negligible, and due to spectroscopy. The spectroscopic error is neglected since most experiments use the same spectroscopic dataset by Wagner and Birk (2003) as will be described below.

3 Comparison with balloon- and airborne measurements: MIPAS-B, Mark IV, FIRS, MIPAS-STR

In this chapter we discuss the comparison of single MIPAS $ClONO_2$ altitude profiles with collocated ones obtained during field campaigns of one aircraft- and various balloon-borne instruments.

For the comparison, the correlative $ClONO_2$ profiles $\boldsymbol{x}_{\mathrm{ref}}$, which, in general, have a better altitude resolution than MIPAS, are adjusted by application of the MIPAS aver-

aging kernel $\mathbf{A}_{\mathrm{MIPAS}}$. Since the a-priori profile of MIPAS retrievals $\boldsymbol{x}_{\mathrm{a,MIPAS}}$ is zero at all altitudes, Eq. (4) of Rodgers and Connor (2003) $\tilde{\boldsymbol{x}}_{\mathrm{ref}}=\boldsymbol{x}_{\mathrm{a,MIPAS}}+\mathbf{A}_{\mathrm{MIPAS}}(\boldsymbol{x}_{\mathrm{ref}}-\boldsymbol{x}_{\mathrm{a,MIPAS}})$ simplifies to

$$\tilde{\boldsymbol{x}}_{\mathrm{ref}} = \mathbf{A}_{\mathrm{MIPAS}}\boldsymbol{x}_{\mathrm{ref}}. \quad (1)$$

Here we assume that the content of the a-priori information in the better resolved correlative profiles is negligibly small (von Clarmann and Grabowski, 2006).

As some of the correlative measurements were not obtained during dedicated validation campaigns with exact matches in time and space we have performed a correction for the profile coincidence error by use of the KASIMA (Karlsruhe Simulation model of the Middle Atmosphere) CTM (Chemical Transport Model) (Kouker et al., 1999). From a multi-annual run with a horizontal resolution of approximately $2.6 \times 2.6^{\circ}$ (T42), a vertical resolution of 0.75 km from 7 to 22 km and an exponential increase above with a resolution of about 2 km in the upper stratosphere, and a model time step of 6 min $ClONO_2$ profiles were interpolated to the time and position of the measurements of the correlative instruments and of MIPAS: $\boldsymbol{x}^{\mathrm{CTM}}_{\mathrm{ref}}$ and $\boldsymbol{x}^{\mathrm{CTM}}_{\mathrm{MIPAS}}$. For the intercomparison, the original MIPAS profiles $\boldsymbol{x}_{\mathrm{MIPAS}}$ were transformed to the time and position of the correlative measurements by adding the difference between the two model results:

$$\boldsymbol{x}^{\mathrm{trans}}_{\mathrm{MIPAS}} = \boldsymbol{x}_{\mathrm{MIPAS}} + \boldsymbol{x}^{\mathrm{CTM}}_{\mathrm{ref}} - \boldsymbol{x}^{\mathrm{CTM}}_{\mathrm{MIPAS}}. \quad (2)$$

The difference profiles $\boldsymbol{x}_{\mathrm{MIPAS}}-\tilde{\boldsymbol{x}}_{\mathrm{ref}}$ and $\boldsymbol{x}^{\mathrm{trans}}_{\mathrm{MIPAS}}-\tilde{\boldsymbol{x}}_{\mathrm{ref}}$ are analysed with regard to systematic altitude dependent biases and the validity of the combined estimated errors.

Below, each instrument (see Table 2 for an overview) and the results of single measurement campaigns will be described in detail. This is followed by a summary of the mean difference profiles per instrument.

3.1 MIPAS-B

MIPAS-B (Table 2) is a balloon-borne limb emission sounder with a similar spectral coverage (4–14 μm), a slightly lower spectral resolution (14.5 cm OPD) and a slightly bet-

ter vertical resolution (2–3 km below the flight level) compared to MIPAS (Friedl-Vallon et al., 2004). The retrieval of $ClONO_2$ vertical profiles from MIPAS-B calibrated spectra is performed with an inversion code based on the same line-by-line radiative transfer model, (KOPRA, Karlsruhe Optimized and Precise Radiative transfer Algorithm, Stiller, 2000) as used in case of MIPAS data evaluation. For inversion of $ClONO_2$ profiles an equivalent scheme as for MIPAS/Envisat with height-constant zero a-priori profile and the same spectroscopic database has been applied (Wetzel et al., 2006; Höpfner et al., 2004).

3.1.1 MIPAS-B: 24 September 2002

During the night 24–25 September 2002 a MIPAS-B balloon flight took place from Aire sur l'Adour in southern France (Oelhaf et al., 2003). This flight was part of the Envisat validation activities and perfectly coincident in time and location to MIPAS measurements of Envisat orbit 2975. Table 3 and Fig. 2 show that the northward-looking MIPAS-B limb scan matches nearly perfectly with the MIPAS profile at 22:07 UT. The southward-looking balloon profile coincides not as perfectly as the northward-looking one with two MIPAS scans: the MIPAS limb-scan at 22:05 is closer below about 24 km altitude while 22:06 is closer above. The bottom panels of Fig. 2 show the comparison of the MIPAS-B and MIPAS profiles. For MIPAS-B, both, the original profile and the profile smoothed with the MIPAS averaging kernel are given. The comparison of MIPAS with the northward-looking MIPAS-B measurement gives the best agreement with maximum differences of 0.12 ppbv at 26 km altitude where MIPAS $ClONO_2$ values are smaller than those of MIPAS-B by about twice the estimated combined total errors. With smaller exceptions at 18 km and at 38 km, the differences are within the estimated error bars. The southern profile of MIPAS-B is within the combined estimated error bounds of either MIPAS scan 22:05 or scan 22:06 almost over the whole altitude region. Only at around 27 km there exist slightly larger absolute differences. At these altitudes the vmr values of MIPAS-B are between those of the two MIPAS limb-scans 22:05 and 22:06.

3.1.2 MIPAS-B: 20/21 March 2003

A further dedicated Envisat validation campaign with MIPAS-B took place above northern Scandinavia on 20/21 March 2003. In the evening of 20 March a coincidence with Envisat orbit 5508 and in the morning of 21 March with orbit 5515 was achieved. MIPAS and MIPAS-B tangent points at and above about 23 km (550 K potential temperature) are located inside the polar vortex while at and below 20 km (475 K) the measurements are located in the vortex edge region. For the evening observation the upper part of the balloon profile (26–31 km) is within the estimated errors of the northern MIPAS scan 21:11, though this is at 30 km altitude about 230 km farther away than scan 21:10 (Fig. 3 and Tab. 3). We attribute this to sampling of different airmasses by MIPAS-B which are more similar to scan 21:11 as indicated by the difference in PV values at 850 K (about 30 km altitude). The PV difference is smallest between balloon and the northern MIPAS scan (Table 3). We cannot prove this assumption by application of the CTM model correction Eq. (2) since this does not change the resulting differences significantly. This might be due to the limited horizontal resolution of the CTM model ($2.6\times2.6^{\circ}$) which does not sufficiently resolve the gradients close to the vortex boundary.

From 25 to 22 km scan 21:10 fits the balloon observation within the combined errors. However, between 18 and 21 km the balloon values are up to 0.25 ppbv lower than those of MIPAS. The reason for this is not clear but might be due to the different direction of the limb-observations at the vortex boundary at these altitudes: while MIPAS looked parallel to the boundary, MIPAS-B looked nearly orthogonal and thus, across stronger gradients in $ClONO_2$.

The comparison on 21 March gives reasonable agreement between the balloon and the nearest MIPAS scan 09:08 above about 22 km. From 19–21 km the maximum difference of 0.14 ppbv is about twice the estimated error. However, in this altitude region a strong south-north gradient of the vmrs is visible in the three MIPAS observations and while MIPAS looked from south to north the viewing direction of MIPAS-B was vice

versa. We suppose that this could be the reason for the observed deviations.

3.1.3 MIPAS-B: 3 July 2003

Another MIPAS-B flight above northern Scandinavia was on 2/3 July. Figure 4 shows the results for two limb-scans measured in different directions with a time delay of about half an hour shortly after mid-night UTC. Both profiles are very similar since, compared to wintertime, there is not much geographical variability of $ClONO_2$ in Arctic summer. Unfortunately there have been no exact matches with MIPAS as shown in Table 3. Best coincidences are in the morning (09:38, 09:39) and in the evening (19:31) of 3 July. Interestingly, MIPAS-B $ClONO_2$ agrees best with the evening scan with differences very close to the combined total errors (Fig. 4, middle). Especially above about 26 km the MIPAS-B and MIPAS evening profiles are systematically higher than the morning measurements. This can be explained by a different exposure to sunlight, thus leading to a different degree of photolysis of $ClONO_2$. While the solar zenith angle during the two MIPAS-B and the MIPAS scan 19:31 was nearly equal with 84–86°, it was 50° and 46° for 09:38 and 09:39, respectively.

Application of the CTM correction led to a significant improvement of the comparison with the MIPAS morning scans (bottom panel of Fig. 4): above about 25 km the large differences have disappeared and the agreement of MIPAS profiles 09:38 and 09:39 with the MIPAS-B observations has become nearly perfect. This result proves our assumption on the effect of $ClONO_2$ photolysis on the comparison.

3.2 Mark IV

The Jet Propulsion Laboratory Mark IV instrument (Toon, 1991) is a balloon-borne Fourier transform infrared interferometer with a very high spectral resolution (57 cm OPD). During sunrise or sunset it measures solar occultation spectra in limb geometry yielding a vertical resolution of about 2 km. Retrieval of trace gas profiles from Mark IV measurements is described by Sen et al. (1998). The Mark IV $ClONO_2$ profiles in

the present study have been retrieved from the ν_4 Q-branch at 780.2 cm^{-1} and the ν_2 Q-branch at 1292.6 cm^{-1}. This is different from the MIPAS, MIPAS-B, MIPAS-STR and FIRS2 data evaluation where only the ν_4 Q-branch region is used. Based on the commonly applied spectroscopic dataset by Wagner and Birk (2003), Oelhaf et al. (2001) have shown that MIPAS-B $ClONO_2$ profiles retrieved from the individual bands agree to within 10%.

3.2.1 Mark IV: 16 December 2002

During the Mark IV flight on 16 December a $ClONO_2$ profile has been obtained during sunrise. The location was inside the polar vortex at each tangent altitude. As shown in Table 4 there was no exact coincidence with MIPAS. Nearest MIPAS profiles have been obtained also inside the vortex in the morning of 15 December (09:24, 09:25) and in the evening of 16 December (18:43). As shown in Fig. 5 the balloon profile is strongly structured with a minimum at around 23 km altitude. This was caused by chlorine activation at polar stratospheric clouds (PSCs) which were abundant in the cold stratosphere in December 2002. Because of PSCs below 24 km MIPAS profiles stop at that altitude for scans 09:24 and 18:43 due to the fact that spectra of PSC-contaminated tangent altitudes are excluded from the data analysis. However, scan 09:25 was PSC free. This scan also shows a $ClONO_2$ minimum similar to Mark IV, which, however, is not as deep due to the worse altitude resolution of MIPAS. This can be seen from the balloon profile convolved with the averaging MIPAS kernel which is much closer to the satellite observation. Somewhat larger differences exist in the regions between 17 and 20 km and 28–30 km. The latter one might be due to some instability of the Mark IV profile which is indicated by comparatively large error bars there. The differences below the minimum are likely due to the complex situation of chlorine activation in the polar vortex. Similar to the comparison with MIPAS-B in March 2003 near the vortex boundary, application of the CTM correction in this case had no significant effect on the comparison.

3.2.2 Mark IV: 1 April 2003

On 1 April 2003 Mark IV measured above northern Scandinavia outside the polar vortex during sunrise at about 03:00 UT. The polar vortex boundary was located about 10° further north. We compare this observation with four closely located MIPAS scans: two in the evening of 31 March (20:24, 20:25) and two in the morning of 1 April (08:20, 08:22) (see Table 4 and Fig. 6). The solar zenith angles were 106° and 102° for the evening observations and 68° and 64° for the morning observations of MIPAS. Photolysis of $ClONO_2$ during daytime is the reason for the better agreement of the balloon measurements with the evening observation (20:24) of MIPAS above about 26 km (middle panel in Fig. 5). This is demonstrated by application of the CTM transformation (bottom panel in Fig. 6). The model correction reduces the differences between the MIPAS morning scans and the Mark IV observation such that the agreement is within the combined error estimates.

3.2.3 Mark IV: 19/20 September 2003

The last Mark IV $ClONO_2$ profile which has been compared to MIPAS was obtained during sunset over the United States on 20 September 2003, 01:28 UT. We compare this with the results from six surrounding limb-scans by MIPAS (Fig. 7) which have been measured 15–17 h (16:47, 16:49, 18:28, 18:29) and 28 h (05:40, 05:42) later. While the profiles closer in time have been obtained during day (SZA: 39–42°) the later ones were measured during night (SZA: 136–140°). General features of the MIPAS profiles are, first, the day-night differences above about 26 km and, second, a northward gradient in the region around the profile maximum during day (16:49 and 18:29 versus 16:47 and 18:28) and night (05:40 versus 05:42) (middle panel in Fig. 7). This gradient and the strong diurnal variations together with the fact that there is no good match make the use of the CTM correction necessary. It results in a much more compact comparison which does not show indications of significant biases (bottom panel of Fig. 7).

3.3 FIRS2

The FIRS-2 instrument is a thermal emission Fourier transform spectrometer operating in the far- (80–340 cm^{-1}) and mid-infrared (330–1220 cm^{-1}) spectral region. Interferograms are recorded with 120 cm OPD. (Johnson et al., 1995). Vertical profiles of $ClONO_2$ volume mixing ratios with an altitude resolution of about 3 km have been derived from FIRS observations using the ν_5 Q-branch at 563 cm^{-1} (Johnson et al., 1996) and the ν_4 Q-branch at 780.2 cm^{-1} (spectroscopic data by Wagner and Birk (2003)).

3.3.1 FIRS2: 19/20 September 2003

On 19/20 September 2003 the FIRS limb-emission instrument provided day- and nighttime profiles of $ClONO_2$. The time and location of these measurements are given in Table 5 and plotted in the top row of Fig. 8. The single balloon results (not shown here) reveal a strong scatter and, especially around 20 km, tend to show negative values. To illustrate the comparison with MIPAS we used the mean day- and nighttime balloon result (red curves in middle row of Fig. 8) which leads to a large scatter of the differences with respect to the single MIPAS profiles. This scatter is reduced by application of the CTM correction (bottom row of Fig. 8). Now, differences are often within the estimated error bars, however, a positive MIPAS bias at 20 km, caused by negative FIRS values there, and a negative bias between 25 and 30 km remain.

3.4 MIPAS-STR

MIPAS-STR is a Fourier transform emission instrument operating in the middle infrared spectral region with similar instrumental specifications as MIPAS-B (see Table 2). During MIPAS validation campaigns MIPAS-STR has been operated from the high-altitude aircraft M55-Geophysica (Keim et al., 2004). One scan of MIPAS-STR consists of limb measurements to get profiles with high vertical resolution below the aircraft and upward observations to obtain limited information about the profile above. Retrieval of $ClONO_2$

profiles from MIPAS-STR calibrated spectra is performed with the same inversion tool and radiative transfer model as used for MIPAS-B data analysis (see above) (Höpfner et al., 2001).

3.4.1 MIPAS-STR: 28 February, 2 and 12 March 2003

During end of February/beginning of March 2003 an Envisat validation campaign with the Geophysica high-altitude aircraft took place from Kiruna in northern Sweden. The MIPAS-STR instrument on-board Geophysica provided measurements of $ClONO_2$ below the aircraft in close coincidence with MIPAS on Envisat during three flights: on 28 February, 2 and 12 March (see Table 6).

The locations of MIPAS-STR and MIPAS observations are given in the top of Figs. 9–11 together with potential vorticity at the 400 K potential temperature level (≈16 km). Following the criterion by Nash et al. (1996), the vortex boundary at this level is about 14 pvu during the three days. Thus, on 28 February the Geophysica measurement corresponding to MIPAS scan 08:25 was inside, while 08:26 was at the inner vortex boundary at 400 K. On 2 March the two southern scans 20:34 and 20:35 were outside, while 20:37 was at the boundary and on 12 March all observations have been inside the polar vortex.

Since a major error source in the MIPAS-STR data analysis is the assumption on the a-priori profile above the aircraft flight level, we show the comparison with MIPAS in Figs. 9–11 for the retrieval with a standard a-priori profile (solid lines) and also with the coincident MIPAS $ClONO_2$ profile as a priori (dashed lines). Using MIPAS results as a-priori leads to a large improvement of the comparison in 4 cases (28Feb08:26, 02Mar20:34, 02Mar20:35, 12Mar08:49), a degradation in one case (28Feb08:25) and no clear change in the other four observations.

3.5 Summary of balloon and airborne profile comparisons

In this section we analyse for each instrument the previously described set of comparisons. For that purpose, mean difference profiles $\bar{\boldsymbol{\delta}}$ have been determined from K single difference profiles: [1]

$$\bar{\boldsymbol{\delta}} = \frac{1}{K}\sum_{k=1}^{K}\boldsymbol{\delta}_k, \tag{3}$$

where $\boldsymbol{\delta}_k = \boldsymbol{x}_{\mathrm{MIPAS},k} - \tilde{\boldsymbol{x}}_{\mathrm{ref},k}$ in case of exactly matching observations and $\boldsymbol{\delta}_k = \boldsymbol{x}^{\mathrm{trans}}_{\mathrm{MIPAS},k} - \tilde{\boldsymbol{x}}_{\mathrm{ref},k}$ in case the CTM model correction has been applied. $\bar{\boldsymbol{\delta}}$ for each instrument is given as solid black curves in the first column of Fig. 12.

For diagnostics, we have calculated the altitude dependent 95% confidence interval of these mean values by

$$\pm 2\boldsymbol{\sigma}_{\bar{\delta},\mathrm{std}} = \pm\sqrt{\frac{1}{K(K-1)}\sum_{k=1}^{K}(\boldsymbol{\delta}_k - \bar{\boldsymbol{\delta}})^2}\;\; t^{-1}_{\mathrm{cdf}}(0.975, K-1) \tag{4}$$

where $t^{-1}_{\mathrm{cdf}}(0.975, K-1)$ is the inverse of the cumulative Student's t-distribution function for $K-1$ degrees of freedom at a value of 97.5% probability.

We have called this interval $\pm 2\boldsymbol{\sigma}_{\bar{\delta},\mathrm{std}}$ since for large sample sizes its limit is ±2 times the standard deviation of the sample divided by the square root of the number of sample elements. The results are shown as dotted black curves in first column of Fig. 12. Green dotted curves in Fig. 12 indicate the range of the estimated total random error of the mean differences ($\pm 2\boldsymbol{\sigma}_{\bar{\delta},\mathrm{err}}$) calculated from the combined error estimation of the

[1] Mind that all variables here are vectors with as many elements as altitude grid points and that the expressions are given per altitude grid point. Thus, K in general is also altitude dependent. Introduction of a further index indicating the altitude dependence is omitted for clarity.

single difference profiles $\sigma_{\bar{\delta},\mathrm{err},k}$ which have already been shown in the discussion of the single profile comparison:

$$\boldsymbol{\sigma}_{\bar{\delta},\mathrm{err}} = \frac{1}{K}\sqrt{\sum_{k=1}^{K}\boldsymbol{\sigma}^2_{\mathrm{err},k}}. \tag{5}$$

Here also the 95% interval is given. In the following we call a bias significant when it is outside these 95% confidence intervals.

For determination of an altitude dependent bias we compare the mean differences to $\pm 2\boldsymbol{\sigma}_{\bar{\delta},\mathrm{std}}$ and $\pm 2\boldsymbol{\sigma}_{\bar{\delta},\mathrm{err}}$. The mean differences between MIPAS and the two instruments MIPAS-B and Mark IV are consistent up to about 32 km altitude: at 15 km MIPAS overestimates $ClONO_2$ vmrs by 0.02–0.03 ppb (up to 100%) and at 20 km by about 0.04–0.05 ppb (up to 15%). From 25 to 32 km there is a slight underestimation of about 0.03 pb (3–4%) for MIPAS-B and a larger one (0.08 ppb, up to 10%) in case of Mark IV. Above, there is a tendency for an overestimation in case of MIPAS-B, but still a clear underestimation (up to 0.1 ppb or 25%) compared to Mark IV. For the MIPAS-B comparisons differences are, however, all within the $\pm 2\boldsymbol{\sigma}_{\bar{\delta},\mathrm{std}}$ interval and, thus, statistically not significant while compared to the estimated errors $\pm 2\boldsymbol{\sigma}_{\bar{\delta},\mathrm{err}}$ the positive MIPAS bias at 15 and 20 km might be real. In case of Mark IV the deviation at high altitudes is clearly significant and the 15 and 20 km differences are just at the limits of the confidence intervals.

Large biases exist in case of the MIPAS-FIRS comparison: from 15–22 km an overestimation of MIPAS up to 0.25 ppb and an underestimation of up to 0.3 ppb in the altitude region 25–31 km. The deviations around 20 km are significant with respect to $\pm 2\boldsymbol{\sigma}_{\bar{\delta},\mathrm{std}}$ and $\pm 2\boldsymbol{\sigma}_{\bar{\delta},\mathrm{err}}$ while at higher altitudes it is within the $\pm 2\boldsymbol{\sigma}_{\bar{\delta},\mathrm{std}}$ interval. We attribute these differences to the FIRS data (1) since these show negative vmrs in the order of 0.2 ppb around 20 km, (2) since during the same measurement campaign in September 2003 the agreement between MIPAS $ClONO_2$ profiles from the same limb scans and the Mark IV observation is much better (see Sect. 3.2.3), and (3) since

there is no indication from any other instrument that these deviations might be due to erroneous MIPAS data.

For the comparison with MIPAS-STR we have chosen those MIPAS-STR retrievals where MIPAS results have been used as a-priori since this seems to reduce the error due to unknown profile shape above the airplane (see Sect. 3.4.1). Results are shown in the bottom row of Fig. 12. Largest differences of about 0.15 ppbv are found at 17 km altitude which are, however, not significant in terms of $\pm 2\sigma_{\bar{\delta},\mathrm{std}}$. The differences are in absolute units larger than in case of the comparison with MIPAS-B or Mark IV. However, in relative units the maximum positive bias is only 13% due to the large values of $ClONO_2$ encountered in the lowermost stratosphere during the MIPAS-STR validation campaign in February/March 2003.

To evaluate the given estimated precision of the measurements without depending on error covariances in the altitude domain, we have calculated χ^2 values of the differences individually per altitude (von Clarmann, 2006):

$$\chi^2 = \sum_{k=1}^{K} \frac{(\delta_k - \bar{\delta})^2}{\sigma_{\mathrm{err},k}^2}. \quad (6)$$

This is compared to the 95% confidence interval of the χ^2 distribution function in the last column of Fig. 12. In this figure all χ^2 values have been divided by $K-1$. In case of MIPAS-B the combined error seems to be underestimated from 16 to 24 km while at higher and lower altitudes it is within the 95% confidence interval. The combined Mark IV-MIPAS error estimation is, with an exception at around 15 km, always at the lower edge of the confidence interval, thus, indicating a slight overestimation of the combined errors. For the comparison with FIRS there is an overestimation of the precision above 32 km and below 15 km while in a large region around 25 km errors seem underestimated. Finally in case of MIPAS-STR the combined random errors are underestimated at 16–17 km altitude while below actual χ^2 values lie inside the 95% confidence interval.

4 Comparison with ground-based measurements: FTIR

We have compared MIPAS $ClONO_2$ observations with ground-based solar absorption FTIR measurements from various stations operating within the Network for the Detection of Atmospheric Composition Change (NDACC, formerly Network for the Detection of Stratospheric Change, NDSC) (see Table 7). From these instruments total column amounts of $ClONO_2$ are available. These data have been derived on the basis of different forward models/inversion schemes (Rinsland et al., 2003; Mellqvist et al., 2002). In the case of Thule observations, the retrieval code SFIT2 (Rinsland et al., 2003) and a two-microwindow approach similar to Reisinger et al. (1995) has been applied. For Izaña measurements PROFFIT (Hase et al., 2004) has been used. In contrast to the scheme described in Rinsland et al. (2003), for Kiruna the approach by Reisinger et al. (1995) has been adopted for the data shown in the present work. Common to the MIPAS data analysis, all FTIR retrievals are performed in the region of the ν_4 Q-branch at 780.2 cm^{-1}, using the spectroscopic data from Wagner and Birk (2003).

For the comparison we have calculated $ClONO_2$ column amounts from the MIPAS profiles using the pressures and temperatures which have been derived from the same spectra in a previous step of the retrieval chain (von Clarmann et al., 2003). These abundances are determined within the available altitude range of MIPAS, i.e. with a maximum coverage of 6–70 km. In the presence of clouds the lower limit is the cloud top derived from MIPAS. Thus, a part of the tropospheric $ClONO_2$ column is missing in the MIPAS derived data but present in the FTIR total columns. In standard profiles of $ClONO_2$ the tropospheric column (0–12 km) is about 1–3% of the total column. Further, some of the FTIR stations used in this intercomparison also derived tropospheric column amount of $ClONO_2$. Mean tropospheric values from these stations lie in the range 0.3%(Wollongong)–2%(Thule) of the total column amount.

The comparisons cover most of the time period of the MIPAS operation discussed in this paper and range from 78.9° N to 45° S (see Fig. 13). The collocated scans of MIPAS with the FTIR measurements have been selected on the basis of a maximum

distance Δd_{max}, time Δt_{max}, and potential vorticity (PV) Δpv_{max} criterion. These criteria have been applied to the locations where the line-of-sight of the FTIRs intersected the altitude of 20 km or the 475 K potential temperature level in case of the PV-criterion, respectively.

Figure 13 shows the comparison of daily mean values for Δd_{max}=800 km, Δt_{max}=8 h, and Δpv_{max}=3×10^{-6} Km^2 kg^{-1} s^{-1}. The data reflect well the annual variation of $ClONO_2$ column amounts with large amplitudes at high-latitude stations (Spitsbergen, Thule, Kiruna, Harestua) in spring. These are due to the chlorine deactivation in stratospheric vortex airmasses, which is even visible at mid-latitudes (Jungfraujoch) on distinct days when vortex air extended far south. Also the annual variation at stations which are rarely affected by vortex air, like Jungfraujoch, Izaña or Lauder, is well met.

For a more detailed investigation, Fig. 14 shows scatter plots for each station and Fig. 15 the histogram of the differences between MIPAS and FTIR. In these Figures black symbols/bars denote the selection for Δd_{max}=800 km, Δt_{max}=8 h, and Δpv_{max}=3×10^{-6} Km^2 kg^{-1} s^{-1} and red symbols/bars the more stringent selection with Δd_{max}=400 km, Δt_{max}=4 h, and Δpv_{max}=3×10^{-6} Km^2 kg^{-1} s^{-1}. Additionally in Table 8 and Table 9 some statistical quantities are listed for the two match cases.

In the following we first analyse the data for any significant bias by comparing the mean difference with their standard deviations. Then estimated errors are discussed with respect to the mean differences and with respect to the derived precision via a χ^2 test.

To decide whether the mean difference $\overline{\delta}$ between MIPAS and FTIR at each station is significant and, thus, might indicate some systematic error, we compare it to the 68% significance interval of the mean difference $\pm\sigma_{\overline{\delta},std}$ from the measurements in Tables 8 and 9. For Δd_{max}=800 km, Δt_{max}=8 h, and Δpv_{max}=3×10^{-6} Km^2 kg^{-1} s^{-1} one station is within $1\sigma_{\overline{\delta},std}$ (Spitsbergen: $-0.37\sigma_{\overline{\delta},std}$), two are within or near 1–$2\sigma_{\overline{\delta},std}$ (Jungfraujoch: $1.75\sigma_{\overline{\delta},std}$, Wollongong: $-2.08\sigma_{\overline{\delta},std}$), four within or near 2–$3\sigma_{\overline{\delta},std}$ (Lauder: $-2.33\sigma_{\overline{\delta},std}$, Izaña: $2.5\sigma_{\overline{\delta},std}$ Kiruna: $2.51\sigma_{\overline{\delta},std}$, Thule: $3.07\sigma_{\overline{\delta},std}$) and one within 3–$4\sigma_{\overline{\delta},std}$ (Harestua: $-3.83\sigma_{\overline{\delta},std}$). For the more stringent match criterion (Table 9) the situation is similar, only that three stations are within 1–$2\sigma_{\overline{\delta},std}$ (Izaña: $1.49\sigma_{\overline{\delta},std}$, Jungfraujoch: $-1.91\sigma_{\overline{\delta},std}$, Thule: $-1.91\sigma_{\overline{\delta},std}$) and four within 2–$3\sigma_{\overline{\delta},std}$ (Lauder: $-2.41\sigma_{\overline{\delta},std}$, Harestua: $-2.51\sigma_{\overline{\delta},std}$, Kiruna: $2.61\sigma_{\overline{\delta},std}$, Wollongong: $-2.86\sigma_{\overline{\delta},std}$) and no one outside $3\sigma_{\overline{\delta},std}$.

The FTIR at Harestua has measured systematically higher values than MIPAS, but only during the summer as indicated by the bi-modal structure of the histogram and the scatter plot. The wintertime data alone show no significant bias. This summertime offset is probably due to a strong dependence of the retrieved column amounts on the assumed a-priori profile in the FTIR retrieval.

In the following, we consider the combined estimated error of MIPAS and the various FTIRs. To calculate the variance $s_{col,noise}$ of the MIPAS derived column amounts due to instrumental noise we applied the linear transformation

$$s_{col,noise} = \rho^T \mathbf{S}_x \rho \quad (7)$$

where $\mathbf{S}_x$ is the covariance matrix of the profile retrieval of $ClONO_2$ volume mixing ratios due to instrumental noise and ρ the vector of the total air partial column amounts. Unlike $\mathbf{S}_x$, which is a regular outcome of the retrieval, an explicit calculation for the other error components is not available for each single $ClONO_2$ profile. To estimate the contribution of these errors we have used the total error calculations which were performed for the MIPAS profiles compared to the collocated profile measurements which have been discussed in Sect. 3 of this paper. As in the case of the profile comparison, the error due to spectroscopic data has been disregarded since all ground-based column observations use the same data as MIPAS. The mean error, excluding noise and spectroscopy, for the vertical column amounts from the 32 single error estimates is 2% with a standard deviation of 2% compared to 5%±4% for the noise error component. Thus, for the total error estimate of MIPAS derived column amounts we have assumed a constant 2% additional random error term for the non-noise and $s_{col,noise}$ for the individual noise error.

Since no specific CTM model results have been available for the MIPAS-FTIR intercomparison a coincidence error component has to be considered additionally (von

Clarmann, 2006). For both coincident criteria we have calculated typical coincidence standard deviations per FTIR station on basis of two datasets: (1) by use of all MIPAS $ClONO_2$ profiles evaluated at IMK for 2002 until 2004 and, (2) by use of KASIMA CTM global fields. Coincidence standard deviations have been determined separately for ±10° latitude bands around each station.

In Tables 8 and 9 we have given the estimated error $\sigma_{\bar{\delta},\mathrm{err,comb}}$ of the mean difference calculated as combined estimated error of MIPAS $\sigma_{\bar{\delta},\mathrm{err,mip}}$, FTIRs $\sigma_{\bar{\delta},\mathrm{err,ftir}}$ and the coincidence error $\sigma_{\bar{\delta},\mathrm{err,coi}}$ under the assumption that all given error terms are of random nature. For $\sigma_{\bar{\delta},\mathrm{err,coi}}$ two values resulting from the different underlying datasets are shown. Since $\sigma_{\bar{\delta},\mathrm{err,comb}}$ values are comparable to $\sigma_{\bar{\delta},\mathrm{std}}$ our conclusions about the mean bias at each station are also valid with regard to the combined estimated errors.

A quantitative analysis of the validity of the precision estimates is gained by the χ^2-test (see Sect. 3.5) presented in the last two columns of Tables 8 and 9. Regarding both matching criteria and the different coincidence error estimates at least two (of four) χ^2 values of Izaña, Jungfraujoch, Thule, Kiruna and Wollongong are within the 95% confidence limit of χ^2. There is indication that the errors for Spitsbergen and Harestua are underestimated while those of Lauder seem to be overestimated.

5 Comparison with spaceborne measurements: ACE-FTS

The Atmospheric Chemistry Experiment (ACE) has been launched into orbit on 13 August 2003 with the solar occultation sounder ACE-FTS (ACE-Fourier Transform Spectrometer) on board. ACE-FTS is a Michelson interferometer which covers the spectral region from 750 to 4400 cm^{-1} with a spectral resolution (maximum optical path difference: 25 cm) (Bernath et al., 2005) slightly higher than that of MIPAS. The retrieval of trace gas profiles from ACE-FTS measurements has been described by Boone et al. (2005).

$ClONO_2$ is derived from the ν_4-Q branch at around 780.2 cm^{-1} for altitudes between 12 and 20 km and from the ν_2-Q branch at around 1292.6 cm^{-1} for altitudes between 18

and 35 km. The spectroscopic data of Wagner and Birk (2003) are used. The vertical resolution of ACE-FTS vmr profiles defined by the field-of-view of the instrument and the tangent altitude spacing is about 3–4 km (Boone et al., 2005) – comparable to that of the MIPAS $ClONO_2$ retrievals. A first comparison of $ClONO_2$ column amounts derived from ACE-FTS vertical profiles and from ground-based solar absorption FTIR measurements in 2004 has been published by Mahieu et al. (2005).

Here we compare $ClONO_2$ profiles from ACE-FTS sunset observations (ACE-FTS level 2 Version 2.2) and MIPAS measurements in the overlapping time period from February 2004, when ACE-FTS regular data collection started, until end of March 2004, when MIPAS nominal mode data ended. For the comparisons we used as match criterion a maximum time difference of 9 h, a maximum tangent point difference of 800 km, and a maximum difference of potential vorticity of 3×10^{-6} $Km^2\,kg^{-1}\,s^{-1}$ at an altitude of 475 K potential temperature. Over all matches, this resulted in a mean distance of 296 km (±154 km), a mean PV difference of -0.007×10^{-6} $Km^2\,kg^{-1}\,s^{-1}$ ($\pm1.49\times10^{-6}$ $Km^2\,kg^{-1}\,s^{-1}$) and a mean time difference of −0.2 h. However, the distribution of the time differences is bi-modal since MIPAS measurements are either at around late morning or early night while ACE-FTS observations are made during sunset. Thus, for comparison with nighttime MIPAS observations the time difference (MIPAS-ACE) is 4–5 h, while in the case of MIPAS daytime measurements it is about −8.1 h at latitudes between 30 and 60° N and −5.6 h for 60–90° N.

In the following, we compare data for these two latitude bands, since sufficient numbers of co-incidences for other regions are not available. The first four rows of Fig. 16 show the comparison for the two latitude bands and MIPAS day/night observations. In the fifth row the combination of all co-incidences is given. In this general case mean differences are less than 0.04 ppbv (less than 5%) up to altitudes of 27 km with MIPAS measuring nearly at all levels higher values than ACE. Mean differences are within the 95% ($\pm2\sigma_{\bar{\delta},\mathrm{std}}$) confidence interval of the mean (black dotted in first column of Fig. 16) from 12.5 to 15 km and from 19 to 22 km with deviations of less than 0.01 ppbv. Above 27 km, differences increase up to nearly 0.15 ppbv or 30% at 34.5 km. Beside this

steady increase there are slightly enhanced differences up to 0.03 ppbv in the range 15–19 km.

The positive MIPAS bias increasing with altitude is present clearly during the night at all latitude bands. At mid-latitudes, however, MIPAS daytime observations are lower than ACE, while nearer to the pole (60–90° N) differences cross from negative to positive values around 25 km and also increase upwards. To investigate, whether photolysis of $ClONO_2$ is the reason for the upper altitude discrepancy we applied KASIMA CTM model simulations provided at all times/locations of MIPAS and ACE-FTS observations. Figure 17 presents the results where the MIPAS profiles have been transformed to the time and location of ACE-FTS by applying Eq. (2).

This transformation affects the comparison primarily at altitudes above about 25 km. In that range the positive MIPAS bias for nighttime observations has been reversed toward a negative bias. This is also the case for the daytime mean profiles at high latitudes above 30 km. For sunlit observations at mid-latitudes the negative bias is reversed to a positive one between 25 and 32 km. In the overall comparison (bottom row in Fig. 17) there is no systematic bias any more up to altitudes of about 27 km. Above 27 km a negative bias of MIPAS with differences up to −0.1 ppbv is present. Thus, maximum absolute differences are reduced by application of the CTM. However, the model overcompensates the photochemically-induced high altitude bias.

The estimated random error $\pm 2\sigma_{\bar{\delta},\mathrm{err}}$ of the mean difference calculated as combined errors from both instruments is given as dotted green curves in the first column of Figs. 16 and 17. While in the upper part of the profile $\pm 2\sigma_{\bar{\delta},\mathrm{err}}$ is comparable to $\pm 2\sigma_{\bar{\delta},\mathrm{std}}$, in the lower part $\pm 2\sigma_{\bar{\delta},\mathrm{err}}$ is smaller. This is reflected in altitude dependent χ^2 values plotted in the fourth column of Figs. 16 and 17. Up to about 23 km χ^2 values are strongly enhanced compared to the 95% confidence interval of χ^2. The fact that there is no significant decrease of the χ^2 profiles when the CTM model correction was applied (Fig. 17 vs. 16) seems to indicate that the observed χ^2 values are not due to coincidence errors. However, (1) the region with high χ^2 is located at altitudes where there are strongly enhanced values of $ClONO_2$ in ACE-FTS and MIPAS profiles due

to chlorine deactivation in spring 2004 and (2) highest χ^2 values are larger in the latitude band nearer to the pole. The CTM model run does not show such large values of $ClONO_2$ in vortex air in February/March 2004. Thus, we suspect that the high χ^2 values are caused by coincidence errors not accounted for by the applied CTM correction.

To test this assumption, as in the case for the ground-based analysis, we determined altitude dependent coincidence errors from (1) MIPAS derived $ClONO_2$ fields in February and March and from (2) KASIMA CTM runs. These have been incorporated in the χ^2 determination (red curves for (1) and green curves for (2) in Figs. 16 and 17). In case of (1) the large χ^2 values disappeared while for (2) there is, on the one hand, a strong reduction above 20 km, but on the other hand, below 20 km χ^2 values stay large. This confirms the view that the underestimated errors are at least partly due to an underestimation of the real $ClONO_2$ variability by the CTM.

6 Conclusions

Vertical profiles of $ClONO_2$ retrieved with the MIPAS level 2 scientific processor at IMK have been validated by comparison with measurements from balloon and aircraft campaigns, with ground-based FTIR data and with satellite observations. Between MIPAS and MIPAS-B observations from dedicated validation campaigns no significant bias has been detected over the whole altitude range from 12 to 39 km. Maximum absolute mean differences are about 0.05 ppbv. The χ^2 test indicates a slight underestimation of the combined estimated error around 20 km altitude. Comparisons to Mark IV observations show no significant bias up to 29 km with absolute differences below 0.05 ppbv. However a slight negative bias between 30 and 35 km of up to −0.1 ppbv (MIPAS-Mark IV) is visible. There is no strong evidence for an error in the precision estimates between the two instruments. Large biases existing between MIPAS and $ClONO_2$ from the flight of the FIRS instrument are very probably caused by the FIRS profiles showing a strong scatter and often negative vmr values. Regarding the dedicated validation measurements of $ClONO_2$ obtained in the lower stratosphere with the airborne MIPAS-

STR, maximum differences are below 0.15 ppbv which are, however, not significant over the whole altitude range from 10–17 km. The combined random error analysis underestimates the precision only between 15 and 17 km.

Comparisons of $ClONO_2$ column amounts from eight ground-based solar absorption FTIR instruments with MIPAS show no evidence for a systematic bias in the MIPAS data. The mean difference (MIPAS-FTIR) at all stations is $0.11\pm0.12\times10^{14}$ cm^{-2} (1.0±1.1%) for a coincidence criterion of Δd_{max}=800 km, Δt_{max}=8 h, and Δpv_{max}=3 × 10^{-6} Km^2 kg^{-1} s^{-1} at 475 K. Application of the stricter criterion Δd_{max}=400 km, Δt_{max}=4 h, and Δpv_{max}=3×10^{-6} Km^2 kg^{-1} s^{-1} at 475 K lead to an overall difference of $-0.09\pm0.19\times10^{14}$ cm^{-2} (−0.8±1.7%). There is no clear evidence for deficiencies in the MIPAS-FTIR combined precision estimates of five instruments while for two the random error seems underestimated and in one case overestimated.

MIPAS profiles of $ClONO_2$ in the period February–March 2003 have been compared to results from the ACE-FTS spaceborne instrument. Up to about 26 km absolute mean differences are below 0.03 ppbv and there is no evidence for a systematic bias between the two datasets. Above this altitude the comparison is aggravated by the diurnal variation of $ClONO_2$ due to photochemistry. This has been shown by application of a chemical transport model which, however, led to an overcorrection of the bias by up to 0.1 ppbv. Such an overcompensation has not been observed in case of the balloon-borne observations of MIPAS-B on 3 July 2003 (Fig. 4), Mark IV on 1 April 2003 (Fig. 6), and Mark IV on 20 September 2003 (Fig. 7) where the CTM correction improved the comparison significantly. Whether the overcorrection in case of the MIPAS-ACE-FTS comparison is caused by a model deficiency or by a remaining bias between the two instruments is an open question. With regard to precision validation, the χ^2 test revealed slight underestimation of the estimated combined precision between MIPAS and ACE-FTS at altitudes above 25 km, but a large underestimation below, with maximum around 18 km. It has been shown that this is likely caused by the large variability of $ClONO_2$ in spring which is not fully reproduced in the CTM model results applied for coincidence error correction.

In summary, this study, which has considered most of the independent measurements of $ClONO_2$ from July 2002 until March 2004, has demonstrated the consistency and reliability of the IMK MIPAS $ClONO_2$ dataset available at (http://www-imk.fzk.de/asf/ame/envisat-data/).

Acknowledgements. Financial support for this project by ESA (contracts 10249/01/NL/SF and 16039/02/NL/SF), the European Union (APE-INFRA: EVR1-CT-1001-40020) and the German Federal Ministry of Education and Research (BMBF 01SF9953/8 and 50EE0203) is gratefully acknowledged. MIPAS spectra were provided by the European Space Agency. The ACE mission is supported by the Canadian Space Agency and the Natural Sciences and Engineering Research Council of Canada. The Belgian contribution has been supported by the ACE and CINAMON Prodex projects (ESA contracts C90207 and C90211, respectively). We also would like to acknowledge the Swedish Environmental Agency and the European Union for funding the measurements at Harestua.

References

Bernath, P. F., McElroy, C. T., Abrams, M. C., Boone, C. D., Butler, M., Camy-Peyret, C., Carleer, M., Clerbaux, C., Coheur, P.-F., Colin, R., DeCola, P., DeMazière, M., Drummond, J. R., Dufour, D., Evans, W. F. J., Fast, H., Fussen, D., Gilbert, K., Jennings, D. E., Llewellyn, E. J., Lowe, R. P., Mahieu, E., McConnell, J. C., McHugh, M., McLeod, S. D., Michaud, R., Midwinter, C., Nassar, R., Nichitiu, F., Nowlan, C., Rinsland, C. P., Rochon, Y. J., Rowlands, N., Semeniuk, K., Simon, P., Skelton, R., Sloan, J. J., Soucy, M.-A., Strong, K., Tremblay, P., Turnbull, D., Walker, K. A., Walkty, I., Wardle, D. A., Wehrle, V., Zander, R., and Zou, J.: Atmospheric Chemistry Experiment (ACE): Mission overview, Geophys. Res. Lett., 32, L15S01, doi:10.1029/2005GL022386, 2005. 9785

Blom, C. E., Fischer, H., Glatthor, N., Gulde, T., Höpfner, M., and Piesch, C.: Spatial and temporal variability of $ClONO_2$, HNO_3 and O_3 in the Arctic winter of 1992/1993 as obtained by airborne infrared emission spectroscopy, J. Geophys. Res., 100, 9101–9114, 1995. 9768

Boone, C. D., Nassar, R., Walker, K. A., Rochon, Y., McLeod, S. D., Rinsland, C. P., and Bernath, P. F.: Retrievals for the atmospheric chemistry experiment Fourier-transform spectrometer, Appl. Opt., 44, 7218–7231, 2005. 9785, 9786

Farmer, C. B., Toon, G. C., Schaper, P. W., Blavier, J.-F., and Lowes, L. L.: Stratospheric trace gases in the spring 1986 Antarctic atmosphere, Nature, 329, 126–130, 1987. 9768

Friedl-Vallon, F., Maucher, G., Kleinert, A., Lengel, A., Keim, C., Oelhaf, H., Fischer, H., Seefeldner, M., and Trieschmann, O.: Design and characterisation of the balloon–borne Michelson Interferometer for Passive Atmospheric Sounding (MIPAS–B2), Appl. Opt., 43, 3335–3355, 2004. 9772

Hase, F., Hannigan, J. W., Coffey, M. T., Goldman, A., Höpfner, M., Jones, N. B., Rinsland, C. P., and Wood, S. W.: Intercomparison of retrieval codes used for the analysis of high-resolution, ground-based FTIR measurements, J. Quant. Spectrosc. Radiat. Transfer, 25–52, 2004. 9782

Höpfner, M., Blom, C. E., von Clarmann, T., Fischer, H., Glatthor, N., Gulde, T., Hase, F., Keim, C., Kimmig, W., Lessenich, K., Piesch, C., Sartorius, C., and Stiller, G. P.: MIPAS–STR data analysis of APE–GAIA measurements, in IRS 2000: Current Problems in Atmospheric Radiation, edited by: Smith, W. L. and Timofeyev, Y. M., 1136–1139, A. Deepak Publishing, Hampton, VA, USA, 2001. 9778

Höpfner, M., von Clarmann, T., Fischer, H., Glatthor, N., Grabowski, U., Kellmann, S., Kiefer, M., Linden, A., Mengistu Tsidu, G., Milz, M., Steck, T., Stiller, G. P., Wang, D.-Y., and Funke, B.: First spaceborne observations of Antarctic stratospheric $ClONO_2$ recovery: Austral spring 2002, J. Geophys. Res., 109, D11308, doi:10.1029/2004JD004609, 2004. 9769, 9770, 9772

Johnson, D. G., Jucks, K. W., Traub, W. A., and Chance, K. V.: Smithsonian stratospheric far-infrared spectrometer and data-reduction system, J. Geophys. Res., 100, 3091–3106, 1995. 9777

Johnson, D. G., Orphal, J., Toon, G. C., Chance, K. V., Traub, W. A., Jucks, K. W., Guelachvili, G., and Morillon-Chapey, M.: Measurement of chlorine nitrate in the stratosphere using the ν_4 and ν_5 bands, Gephys. Res. Lett., 23, 1745–1748, 1996. 9777, 9797

Keim, C., Blom, C. E., von der Gathen, P., Gulde, T., Höpfner, M., Liu, G. Y., Oulanovski, A., Piesch, C., Ravegnani, F., Sartorius, C., Schlager, H., and Volk, C. M.: Validation of MIPAS-ENVISAT by correlative measurements of MIPAS-STR, in Proc. ACVE-2 Validation Workshop, 3–7 May, 2004, ESRIN, Frascati, Italy, vol. SP-562, ESA Publications Division, ESTEC, Postbus 299, 2200 AG Noordwijk, The Netherlands, 2004. 9777

Kouker, W., Langbein, I., Reddmann, T., and Ruhnke, R.: The Karlsruhe simulation model of the middle atmosphere (KASIMA), version 2, vol. FZKA 6278 of Wissenschaftliche Berichte,

Forschungszentrum Karlsruhe, 1999. 9771

Mahieu, E., Zander, R., Duchatelet, P., Hannigan, J. W., Coffey, M. T., Mikuteit, S., Hase, F., Blumenstock, T., Wiacek, A., Strong, K., Taylor, J. R., Mittermeier, R. L., Fast, H., Boone, C. D., McLeod, S. D., Walker, K. A., Bernath, P. F., and Rinsland, C. P.: Comparisons between ACE-FTS and ground-based measurements of stratospheric HCl and $ClONO_2$ loadings at northern latitudes, Geophys. Res. Lett., 32, L15S08, doi:10.1029/2005GL022396, 2005. 9786

Marcy, T. P., Gao, R., Northway, M. J., Popp, P. J., Stark, H., and Fahey, D.: Using chemical ionization mass spectrometry for detection of HNO_3, HCl, and $ClONO_2$ in the atmosphere, Int. J. Mass Spectrom., 243, 63–70, 2005. 9768

Mellqvist, J., Galle, B., Blumenstock, T., Hase, F., Yashcov, D., Notholt, J., Sen, B., Blavier, J.-F., Toon, G. C., and Chipperfield, M. P.: Ground-based FTIR observations of chlorine activation and ozone depletion inside the Arctic vortex during the winter of 1999/2000, J. Geophys. Res. (Atmos.), 107, 6–1, 2002. 9782

Mergenthaler, J. L., Kumer, J. B., Roche, A. E., Nightingale, R. W., Potter, J. F., Gille, J. C., Massie, S. T., Bailey, P. L., Edwards, D., Connell, P. S., Kinnison, D. E., Gunson, M. R., Abrams, M. C., Toon, G. C., Sen, B., Blavier, J.-F., Murcray, D. G., Murcray, F. J., and Goldman, A.: Validation of CLAES $ClONO_2$ measurements, J. Geophys. Res., 101, 9603–9620, 1996. 9768

Murcray, D. G., Goldman, A., Murcray, F. H., Murcray, F. J., and Williams, W. J.: Stratospheric Distribution of $ClONO_2$, Geophys. Res. Lett., 6, 857–859, 1979. 9768

Nash, E. R., Newmann, P. A., Rosenfield, J. E., and Schoeberl, M. R.: An objective determination of the polar vortex using Ertel's potential vorticity, J. Geophys. Res., 101, 9471–9478, 1996. 9778, 9807, 9809

Norton, H. and Beer, R.: New apodizing functions for Fourier spectrometry, J. Opt. Soc. Am., 66, 259–264, (Errata J. Opt. Soc. Am., 67, 419, 1977), 1976. 9769

Oelhaf, H., Clarmann, T. V., Fischer, H., Friedl-Vallon, F., Fritzsche, C., Linden, A., Piesch, C., Seefeldner, M., and Völker, W.: Stratospheric $ClONO_2$ and HNO_3 profiles inside the Arctic vortex from MIPAS-B limb emission spectra obtained during EASOE, Geophys. Res. Lett., 21, 1263–1266, 1994. 9768

Oelhaf, H., Wetzel, G., Höpfner, M., Friedl-Vallon, F., Glatthor, N., Maucher, G., Stiller, G., Trieschmann, O., von Clarmann, T., Birk, M., and Wagner, G.: Interconsistency Checks of $ClONO_2$ Retrievals from MIPAS–B Spectra by using different Bands and spectroscopic

Parameter Sources, in: IRS 2000: Current Problems in Atmospheric Radiation, edited by: Smith, W. L. and Timofeyev, Y. M., 615–618, A. Deepak Publishing, Hampton, VA, USA, 2001. 9775

Oelhaf, H., Friedl-Vallon, F., Kleinert, A., Lengel, A., Maucher, G., Nordmeyer, H., Wetzel, G., Zhang, G., and Fischer, H.: ENVISAT validation with MIPAS–B, in: Proc. ENVISAT Validation Workshop, 9–13 December, 2002, ESRIN, Frascati, Italy, CD-ROM, vol. SP-531, ESA Publications Division, ESTEC, Postbus 299, 2200 AG Noordwijk, The Netherlands, 2003. 9772

Reisinger, A. R., Jones, N. B., Matthews, W. A., and Rinsland, C. P.: Southern hemisphere midlatitude ground-based measurements of $ClONO_2$: Method of analysis, seasonal cycle and long term-trend, J. Geophys. Res., 100, 23 183–23 193, 1995. 9782

Rinsland, C. P., Goldman, A., Murcray, D. G., Murcray, F. J., and Malathy Devi, V.: Tentative identification of the 780 cm^{-1} ν_4 band Q branch of chlorine nitrate in high-resolution solar absorption spectra of the stratosphere, J. Geophys. Res., 90, 7931–7943, 1985. 9768

Rinsland, C. P., Gunson, M. R., Abrams, M. C., Zander, R., Mahieu, E., Goldman, A., Ko, M. K. W., Rodriguez, J. M., and Sze, N. D.: Profiles of stratospheric chlorine nitrate ($ClONO_2$) from atmospheric trace molecule spectroscopy/ATLAS 1 infrared solar occultation spectra, J. Geophys. Res., 99, 18 895–18 900, 1994. 9768

Rinsland, C. P., Gunson, M. R., Abrams, M. C., Lowes, L. L., Zander, R., Mahieu, E., Goldman, A., and Irion, F. W.: April 1993 Arctic profiles of stratospheric HCl, $ClONO_2$, and CCl_2F_2 from atmospheric trace molecule spectroscopy/ATLAS 2 infrared solar occultation spectra, J. Geophys. Res., 100, 14 019–14 028, 1995. 9768

Rinsland, C. P., Gunson, M. R., Salawitch, R. J., Michelsen, H. A., Zander, R., Newchurch, M. J., Abbas, M. M., Abrams, M. C., Manney, G. L., Chang, A. Y., Irion, F. W., Goldman, A., and Mahieu, E.: ATMOS/ATLAS-3 measurements of stratospheric chlorine and reactive nitrogen partitioning inside and outside the November 1994 Antarctic vortex, Geophys. Res. Lett., 23, 2365–2368, 1996. 9768

Rinsland, C. P., Mahieu, E., Zander, R., Jones, N. B., Chipperfield, M. P., Goldman, A., Anderson, J., Russell III, J. M., Demoulin, P., Notholt, J., Toon, G. C., Blavier, J.-F., Sen, B., Sussmann, R., Wood, S. W., Meier, A., Griffith, D. W. T., Chiou, L. S., Murcray, F. J., Stephen, T. M., Hase, F., Mikuteit, S., Schulz, A., and Blumenstock, T.: Long–term trends of inorganic chlorine from ground–based infrared solar spectra: Past increases and evidence for stabilization, J. Geophys. Res., 108, 4252, doi:10.1029/2002JD003001, 2003. 9782

Roche, A. E., Kumer, J. B., and Mergenthaler, J. L.: CLAES observations of $ClONO_2$ and HNO_3 in the antarctic stratosphere, between June 15 and September 17, 1992, Geophys. Res. Lett., 20, 1223–1226, 1993. 9768

Roche, A. E., Kumer, J. B., Mergenthaler, J. L., Nightingale, R. W., Uplinger, W. G., Ely, G. A., Potter, J. F., Wuebbles, D. J., Connell, P. S., and Kinnison, D. E.: Observations of Lower-Stratospheric $ClONO_2$, HNO_3, and Aerosol by the UARS CLAES Experiment between January 1992 and April 1993., J. Atmos. Sci., 51, 2877–2902, 1994. 9768

Rodgers, C. D.: Inverse Methods for Atmospheric Sounding: Theory and Practice, vol. 2 of Series on Atmospheric, Oceanic and Planetary Physics, edited by: Taylor, F. W., World Scientific, 2000. 9770

Rodgers, C. D. and Connor, B. J.: Intercomparison of remote sounding instruments, J. Geophys. Res., 108, 4116, doi:10.1029/2002JD002299, 2003. 9771

Sen, B., Toon, G. C., Osterman, G. B., Blavier, J.-F., Margitan, J. J., Salawitch, R. J., and Yue, G. K.: Measurements of reactive nitrogen in the stratosphere, J. Geophys. Res., 103, 3571–3586, 1998. 9774

Solomon, S.: Stratospheric Ozone Depletion: A Review of Concepts and History, Rev. Geophys., 37, 275–315, 1999. 9768

Stiller, G. P. (Ed.): The Karlsruhe Optimized and Precise Radiative Transfer Algorithm (KOPRA), vol. FZKA 6487 of Wissenschaftliche Berichte, Forschungszentrum Karlsruhe, 2000. 9772

Stimpfle, R. M., Cohen, R. C., Bonne, G. P., Voss, P. B., Perkins, K. K., Koch, L. C., Anderson, J. G., Salawitch, R. J., Lloyd, S. A., Gao, R. S., DelNegro, L. A., Keim, E. R., and Bui, T. P.: The coupling of $ClONO_2$, ClO, and NO_2 in the lower stratosphere from in situ observations using the NASA ER–2 aircraft, J. Geophys. Res., 104, 26 705–26 714, 1999. 9768

Toon, G. C.: The JPL MkIV Interferometer, Opt. Photonics News, 2, 19–21, 1991. 9774

von Clarmann, T.: Validation of remotely sensed profiles of atmospheric state variables: strategies and terminology, Atmos. Chem. Phys. Discuss., 6, 4973–4994, 2006. 9781, 9784

von Clarmann, T. and Grabowski, U.: Elimination of hidden a priori information from remotely sensed profile data, Atmos. Chem. Phys. Discuss., 6, 6723–6751, 2006. 9771

von Clarmann, T., Fischer, H., Friedl-Vallon, F., Linden, A., Oelhaf, H., Piesch, C., Seefeldner, M., and Völker, W.: Retrieval of stratospheric O_3, HNO_3, and $ClONO_2$ profiles from 1992 MIPAS-B limb emission spectra: method, results, and error analysis, J. Geopyhs. Res., 98, 20 495–20 506, 1993. 9768

von Clarmann, T., Glatthor, N., Grabowski, U., Höpfner, M., Kellmann, S., Kiefer, M., Linden, A., Mengistu Tsidu, G., Milz, M., Steck, T., Stiller, G. P., Wang, D. Y., Fischer, H., Funke, B., Gil-López, S., and López-Puertas, M.: Retrieval of temperature and tangent altitude pointing from limb emission spectra recorded from space by the Michelson Interferometer for Passive Atmospheric Sounding (MIPAS), J. Geophys. Res., 108, 4736, doi:10.1029/2003JD003602, 2003. 9782

Wagner, G. and Birk, M.: New spectroscopic database for chlorine nitrate, J. Quant. Spectrosc. Radiat. Transfer, 82, 381–407, 2003. 9770, 9775, 9777, 9782, 9786, 9796, 9797

Wetzel, G., Oelhaf, H., Friedl-Vallon, F., Kleinert, A., Lengel, A., Maucher, G., Nordmeyer, H., Ruhnke, R., Nakajima, H., Sasano, Y., Sugita, T., and Yokota, T.: Intercomparison and validation of ILAS-II version 1.4 target parameters with MIPAS-B measurements, J. Geophys. Res., 111, D11S06, doi:10.1029/2005JD006287, 2006. 9772

Zander, R. and Demoulin, P.: Spectroscopic evidence for the presence of the ν_4 - Q branch of chlorine nitrate ($ClONO_2$) in ground-based infrared solar spectra, J. Atmos. Chem., 6, 191–200, 1988. 9768

Zander, R., Rinsland, C. P., Farmer, C. B., Brown, L. R., and Norton, R. H.: Observation of several chlorine nitrate ($ClONO_2$) bands in stratospheric infrared spectra, Geophys. Res. Lett., 13, 757–760, 1986. 9768

Zander, R., Mahieu, E., Gunson, M. R., Abrams, M. C., Chang, A. Y., Abbas, M., Aellig, C., Engel, A., Goldman, A., Irion, F. W., Kämpfer, N., Michelsen, H. A., Newchurch, M. J., Rinsland, C. P., Salawitch, R. J., Stiller, G. P., and Toon, G. C.: The 1994 northern midlatitude budget of stratospheric chlorine derived from ATMOS/ATLAS-3 observations, Geophys. Res. Lett., 23, 2357–2360, 1996. 9768

Table 1. Error budget at selected altitudes for the retrieval of $ClONO_2$ from MIPAS limb-scan on 24 September 2002, 22:07 UTC at 46.1° N/0.6° E. The absolute errors in pptv are given outside and the relative errors (%) inside the brackets.

Height [km]	Total Error[a]	Instrument Noise	Interf. gases[b]	Temp.[c]	Temp. gradient[d]	Pointing[e]	Spectro. data[f]	Gain[g]	ILS[h]	Spect. shift[i]	Non-LTE[j]
11	18(321)	17(300)	<1(10)	2(41)	<1(7)	5(92)	3(53)	<1(7)	1(23)	<1(<1)	<1(<1)
14	24(118)	24(116)	<1(4)	2(10)	<1(1)	2(9)	3(15)	<1(1)	<1(<1)	<1(<1)	<1(<1)
17	34(32)	33(31)	<1(<1)	2(2)	<1(<1)	8(7)	1(<1)	<1(<1)	1(1)	<1(<1)	<1(<1)
20	45(13)	41(12)	1(<1)	<1(<1)	<1(<1)	12(3)	14(4)	2(<1)	5(1)	3(<1)	<1(<1)
23	61(7)	49(6)	3(<1)	5(<1)	<1(<1)	3(<1)	34(4)	<1(<1)	10(1)	6(<1)	<1(<1)
26	75(7)	55(5)	3(<1)	8(<1)	<1(<1)	7(<1)	47(5)	<1(<1)	13(1)	10(<1)	<1(<1)
29	89(7)	60(5)	5(<1)	12(<1)	1(<1)	23(2)	55(4)	2(<1)	15(1)	17(1)	1(<1)
32	97(10)	68(7)	5(<1)	13(1)	1(<1)	34(3)	51(5)	3(<1)	16(2)	22(2)	<1(<1)
35	91(12)	73(9)	10(1)	7(<1)	<1(<1)	28(4)	44(6)	1(<1)	7(<1)	4(<1)	<1(<1)
38	89(21)	78(19)	10(2)	1(<1)	2(<1)	10(2)	34(8)	<1(<1)	3(<1)	21(5)	<1(<1)
41	103(26)	95(24)	5(1)	9(2)	4(<1)	9(2)	22(5)	2(<1)	14(3)	28(7)	<1(<1)

[a] Defined as quadratic sum of all individual errors. [b] The variability of the interfering gases which where not jointly fitted is assumed on basis of their climatological variability. [c] Based on temperature uncertainty of 1 K. [d] Estimated errors due to horizontal inhomogeneities of temperature of 0.01 K/km. For standard processing horizontal inhomogeneities were neglected in $ClONO_2$ retrievals. [e] Based on tangent altitude uncertainty of 150 m. [f] Based on uncertainty of spectroscopic data of 5% (worst case) for $ClONO_2$ (Wagner and Birk, 2003) and information by J. M. Flaud, personal communication, 2003). [g] Based on gain calibration error of 1%. [h] Based on an error of the assumed instrumental line-shape of 3%. [i] Based on a residual spectral shift error of 0.0005 cm^{-1}. [j] Model error based on radiative transfer calculations including non-local thermodynamic equilibrium (non-LTE) versus calculations without considering non-LTE. For standard processing non-LTE was neglected in $ClONO_2$ retrievals.

Table 2. Comparison of instrumental and data processing details of measurement systems of $ClONO_2$ vertical profiles addressed in this study.

Instrument	MIPAS	MIPAS-B	Mark IV	FIRS2	MIPAS-STR	ACE-FTS
Platform	Satellite	Balloon	Balloon	Balloon	Aircraft	Satellite
Observation geometry	limb	limb	limb	limb	limb+upward	limb
Observation mode	emission	emission	solar occultation	emission	emission	solar occultation
Vertical resolution [km]	3–4	2–3	2	3	2	3
Spectral resolution (unapodised) [cm^{-1}]	0.025	0.035	0.009	0.004	0.035	0.02
$ClONO_2$ window:						
ν_5 Q-branch at 563 cm^{-1}	no	no	no	yes	no	no
ν_4 Q-branch at 780.2 cm^{-1}	yes	yes	yes	yes	yes	yes
ν_2 Q-branch at 1292.6 cm^{-1}	no	no	yes	no	no	yes
Spectroscopy:						
Johnson et al. (1996)	no	no	no	yes	no	no
Wagner and Birk (2003)	yes	yes	yes	yes	yes	yes

Table 3. Details for profile intercomparison during MIPAS-B campaigns on 24 September 2002, 20/21 March 2003, and 3 July 2003.

MIPAS-B Date/time UTC	lat/lon @20 km	lat/lon @30 km	MIPAS date/time UTC	lat/lon @20 km	lat/lon @30 km	Δt [h]	Δd[km] @20 km	Δd[km] @30 km	ΔPV @475 K	ΔPV @850 K
24SEP/22:25	47.5/0.6	46.2/0.8	24SEP/22:07	46.8/0.6	46.1/0.6	–0.3	72	10	0	3
24SEP/21:45	38.9/1.1	40.2/1.0	24SEP/22:05	37.4/2.5	36.7/2.6	0.3	208	405	–2	–7
			24SEP/22:06	42.1/1.5	41.4/1.6	0.4	355	149	3	12
20MAR/20:55	65.7/13.9	66.6/19.7	20MAR/21:08	61.7/15.1	61.0/15.2	0.2	448	657	–2	171
			20MAR/21:10	66.4/14.1	65.7/14.1	0.3	80	268	1	205
			20MAR/21:11	71.2/14.1	70.5/14.1	0.3	617	496	2	96
21MAR/08:47	64.8/16.7	67.2/18.7	21MAR/09:06	69.8/18.4	70.5/18.8	0.3	560	368	4	70
			21MAR/09:08	65.0/16.7	65.7/17.0	0.3	25	179	0	71
			21MAR/09:09	60.3/15.3	60.9/15.6	0.4	511	709	–2	184
03JUL/00:33	70.6/28.5	69.6/25.6	03JUL/09:38	69.9/10.5	70.5/10.9	9.1	681	565	-1	3
			03JUL/09:39	65.1/8.8	65.8/9.1	9.1	1020	815	–1	12
			03JUL/19:31	71.2/39.3	70.5/39.3	19.0	396	523	1	–9
03JUL/01:06	69.7/8.1	69.1/12.0	03JUL/09:38	69.9/10.5	70.5/10.9	8.5	93	161	0	–4
			03JUL/09:39	65.1/8.8	65.8/9.1	8.6	508	392	0	6
			03JUL/19:31	71.2/39.3	70.5/39.3	18.4	1158	1048	3	-16

Table 4. Details for profile intercomparison during Mark IV campaigns on 16 December 2002, 1 April 2003, and 20 September 2003.

Mark IV Date/time UTC	lat/lon @20 km	lat/lon @30 km	MIPAS date/time UTC	lat/lon @20 km	lat/lon @30 km	Δt [h]	Δd[km] @20 km	Δd[km] @30 km	ΔPV @475 K	ΔPV @850 K
16DEC/08:10	64.4/31.2	66.7/30.7	15DEC/09:24	69.7/14.0	70.4/14.4	–22.8	944	774	2	149
			15DEC/09:25	65.0/12.3	65.6/12.7	–22.7	894	815	–2	12
			16DEC/18:43	66.5/50.7	65.8/50.8	10.6	929	901	2	–36
01APR/02:58	68.3/35.3	67.7/30.7	31MAR/20:24	66.4/25.6	65.7/25.6	–6.6	467	312	2	35
			31MAR/20:25	71.2/25.6	70.5/25.6	–6.6	492	380	–1	–57
			01APR/08:20	69.8/29.9	70.5/30.3	5.4	273	314	1	–68
			01APR/08:22	65.0/28.2	65.7/28.5	5.4	477	237	2	–26
20SEP/01:28	34.3/-113.3	34.2/-111.3	20SEP/16:47	35.5/-98.2	36.2/–98.0	15.3	1381	1225	–2	38
			20SEP/16:49	30.7/–99.5	31.4/–99.3	15.3	1359	1169	–2	–21
			20SEP/18:28	35.5/–123.4	36.2/–123.2	17.0	926	1098	1	–9
			20SEP/18:29	30.7/–124.6	31.4/–124.4	17.0	1129	1262	–2	–8
			21SEP/05:40	31.4/–112.6	30.7/–112.5	28.2	325	401	0	–22
			21SEP/05:42	37.3/–111.7	36.6/–111.6	28.2	369	272	4	42

Table 5. Details of FIRS2 profile locations 19/20 September 2003.

FIRS2 Date/time UTC	lat/lon 20 km	lat/lon 30 km
19SEP/18:00	31.6/–108.6	32.4/–107.5
19SEP/20:22	37.5/–109.4	36.7/–108.4
19SEP/22:08	38.2/–105.2	37.1/–105.6
19SEP/23:49	37.3/–110.5	36.5/–109.6
20SEP/02:49	32.7/–112.8	33.2/–111.3
20SEP/04:56	29.5/–110.2	25.8/–147.2
20SEP/07:18	32.6/–113.9	22.3/–178.1
20SEP/09:22	29.8/–113.2	31.1/–113.0

Table 6. Details for profile intercomparison during MIPAS-STR campaigns on 28 February, 2 March, and 12 March 2003.

MIPAS-STR Date/time UTC	lat/lon @16 km	MIPAS date/time UTC	lat/lon @16 km	Δt [h]	Δd[km] @16 km	ΔPV @400 K
28FEB/07:56	69.7/22.8	28FEB/08:26	69.6/28.3	0.5	212	1
28FEB/08:59	75.3/28.7	28FEB/08:25	74.9/30.9	–0.6	79	0
02MAR/19:20	66.6/23.7	02MAR/20:35	66.6/22.7	1.2	42	0
02MAR/20:30	61.8/24.7	02MAR/20:34	61.9/23.7	0.1	52	0
02MAR/22:08	70.9/26.8	02MAR/20:37	71.5/22.8	–1.5	157	–1
12MAR/07:59	69.6/18.6	12MAR/08:49	69.6/22.5	0.8	151	–1
12MAR/08:55	75.2/21.2	12MAR/08:48	74.9/25.1	–0.1	114	0
12MAR/09:17	78.3/17.7	12MAR/08:46	79.6/22.8	–0.5	179	0
12MAR/09:56	75.1/4.3	12MAR/10:28	74.9/-0.0	0.5	126	–2

Table 7. NDACC stations used for comparisons with MIPAS.

Station	Latitude	Longitude	Altitude [km]
Spitsbergen	78.92° N	11.93° E	0.02
Thule	76.53° N	68.74° W	0.03
Kiruna	67.84° N	20.41° E	0.42
Harestua	60.21° N	10.75° E	0.60
Jungfraujoch	46.55° N	7.98° E	3.58
Izaña	28.3° N	16.48° W	2.37
Wollongong	34.4° S	150.9° E	0.03
Lauder	45.04° S	169.68° E	0.37

Table 8. Statistics of MIPAS-FTIR differences. The collocation criterion is Δd_{max}=800 km, Δt_{max}=8 h, and Δpv_{max}=3×10^{-6} Km^2 kg^{-1} s^{-1} at 475 K. Unless noted with [n.u.], values are given in units of 10^{14} cm^{-2}. Number of samples: n. Mean difference of column amounts MIPAS-FTIR: $\bar{\delta}$. Standard deviation of the differences: σ_{std}. 68% confidence level of $\bar{\delta}$: $\sigma_{\bar{\delta},std}$. Estimated error contribution of $\bar{\delta}$ by MIPAS: $\sigma_{\bar{\delta},err,mip}$. Estimated error contribution of $\bar{\delta}$ by FTIR: $\sigma_{\bar{\delta},err,ftir}$. Estimated coincidence error contribution of $\bar{\delta}$; without brackets: based on MIPAS statistics, in brackets: based on KASIMA CTM statistics: $\sigma_{\bar{\delta},err,coi}$. Combined estimated error of $\bar{\delta}$; without brackets: calculated with $\sigma_{\bar{\delta},err,coi}$ from MIPAS statistics, in brackets: based on $\sigma_{\bar{\delta},err,coi}$ from KASIMA CTM statistics: $\sigma_{\bar{\delta},err,comb}$. χ^2 value; without brackets: calculated with $\sigma_{\bar{\delta},err,coi}$ from MIPAS statistics, in brackets: based on $\sigma_{\bar{\delta},err,coi}$ from KASIMA CTM statistics: χ^2. 95% confidence interval of χ^2: χ^2 95% range.

Station	n [n.u.]	$\bar{\delta}$	σ_{std}	$\sigma_{\bar{\delta},std}$	$\sigma_{\bar{\delta},err,mip}$	$\sigma_{\bar{\delta},err,ftir}$	$\sigma_{\bar{\delta},err,coi}$	$\sigma_{\bar{\delta},err,comb}$	χ^2 [n.u.]	χ^2 95% range [n.u.]
Spitsbergen	15	–0.41 (–3.0%)	4.16	1.12	0.07	0.41	0.56 (0.46)	0.70 (0.62)	2.66 (3.49)	0.40–1.87
Thule	60	1.38 (10.1%)	3.45	0.45	0.05	0.50	0.28 (0.23)	0.57 (0.55)	0.80 (0.95)	0.67–1.39
Kiruna	93	0.74 (6.1%)	2.82	0.29	0.05	0.09	0.21 (0.22)	0.23 (0.24)	1.78 (1.56)	0.73–1.31
Harestua	69	–1.24 (–9.2%)	2.67	0.32	0.05	0.08	0.19 (0.25)	0.22 (0.27)	2.23 (1.41)	0.69–1.36
Jungfraujoch	70	0.40 (4.1%)	1.92	0.23	0.05	0.12	0.16 (0.22)	0.21 (0.25)	1.22 (0.82)	0.69–1.36
Izana	85	0.60 (10.6%)	2.20	0.24	0.05	0.19	0.14 (0.15)	0.24 (0.25)	0.96 (0.87)	0.72–1.32
Wollongong	30	–0.89 (–9.6%)	2.31	0.43	0.09	0.28	0.16 (0.18)	0.34 (0.35)	2.00 (1.84)	0.55–1.58
Lauder	112	–0.50 (–5.5%)	2.24	0.21	0.04	0.32	0.11 (0.09)	0.34 (0.33)	0.42 (0.44)	0.75-1.28

Table 9. Same as Table 8 but for the more stringent collocation criterion: Δd_{max}=400 km, Δt_{max}=4 h, and Δpv_{max}=3×10^{-6} Km^2 kg^{-1} s^{-1} at 475 K.

Station	n [n.u.]	$\bar{\delta}$	σ_{std}	$\sigma_{\bar{\delta},std}$	$\sigma_{\bar{\delta},err,mip}$	$\sigma_{\bar{\delta},err,ftir}$	$\sigma_{\bar{\delta},err,coi}$	$\sigma_{\bar{\delta},err,comb}$	χ^2 [n.u.]	χ^2 95% range [n.u.]
Spitsbergen	12	0.13 (0.9%)	3.81	1.15	0.15	0.43	0.34 (0.38)	0.57 (0.59)	4.53 (4.10)	0.35–1.99
Thule	48	0.89 (6.9%)	3.21	0.47	0.10	0.52	0.15 (0.19)	0.55 (0.56)	1.38 (1.21)	0.64–1.44
Kiruna	41	0.99 (8.3%)	2.40	0.38	0.09	0.12	0.29 (0.28)	0.32 (0.32)	1.36 (1.37)	0.61–1.48
Harestua	33	–1.45 (–10.8%)	3.26	0.58	0.10	0.12	0.24 (0.31)	0.28 (0.35)	3.99 (2.58)	0.57–1.55
Jungfraujoch	20	-0.68 (–6.2%)	1.55	0.36	0.14	0.26	0.24 (0.34)	0.38 (0.44)	0.74 (0.54)	0.47–1.73
Izana	17	0.46 (9.0%)	1.24	0.31	0.10	0.36	0.25 (0.15)	0.45 (0.40)	0.48 (0.68)	0.43–1.80
Wollongong	7	–2.02 (–20.4%)	1.71	0.71	0.25	0.55	0.14 (0.19)	0.62 (0.63)	0.90 (0.80)	0.21–2.41
Lauder	45	–0.83 (-8.9%)	2.27	0.34	0.09	0.52	0.13 (0.13)	0.54 (0.54)	0.49 (0.49)	0.63–1.46

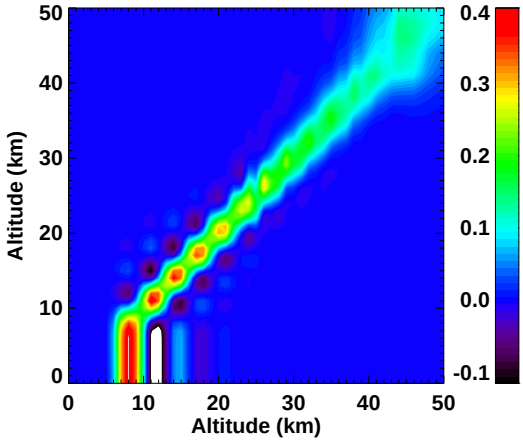

Fig. 1. Averaging kernel of $ClONO_2$ retrieval from MIPAS limb-scan on 24 September 2002, 22:07 UTC at 46.1° N/0.6° E (Best coincidence with MIPAS-B: Table 3 and Fig. 2).

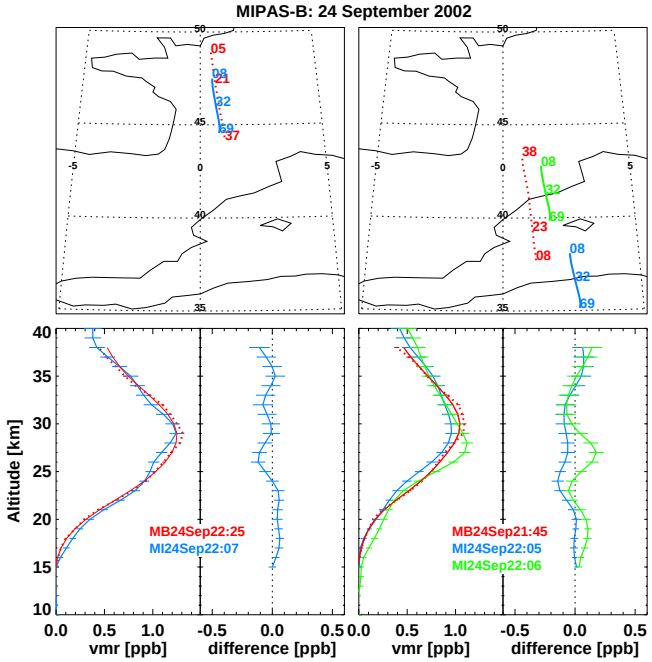

Fig. 2. Top: location of MIPAS-B (red) and MIPAS (other colours) limb scans for the validation campaign on 24 September 2002. The numbers indicate the positions of selected tangent points. Bottom panels left part: Retrieved altitude profiles of $ClONO_2$ from MIPAS-B (dotted, red, $\boldsymbol{x}_{\text{ref}}$ in Eq. 1) and MIPAS (solid, other colours, $\boldsymbol{x}_{\text{MIPAS}}$). The solid red lines are the MIPAS-B observations smoothed by the MIPAS averaging kernel ($\tilde{\boldsymbol{x}}_{\text{ref}}$). Bars indicate estimated total random errors. Bottom panels right part: Difference profiles $\boldsymbol{x}_{\text{MIPAS}} - \tilde{\boldsymbol{x}}_{\text{ref}}$ and combined total errors for each MIPAS scan.

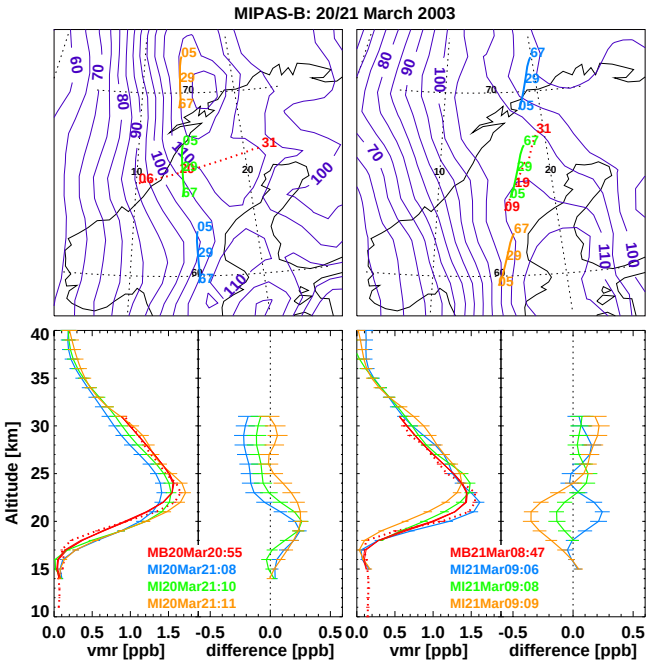

Fig. 3. Same as Fig. 2 but for the validation campaign on 20/21 March 2003. Blue contour lines in the maps show the fields of potential vorticity (PV) (units: $\mathrm{K\,m^2\,kg^{-1}\,s^{-1}}$) at 550 K potential temperature. Using the criterion by Nash et al. (1996) the vortex boundary is located at $70\,\mathrm{K\,m^2\,kg^{-1}\,s^{-1}}$.

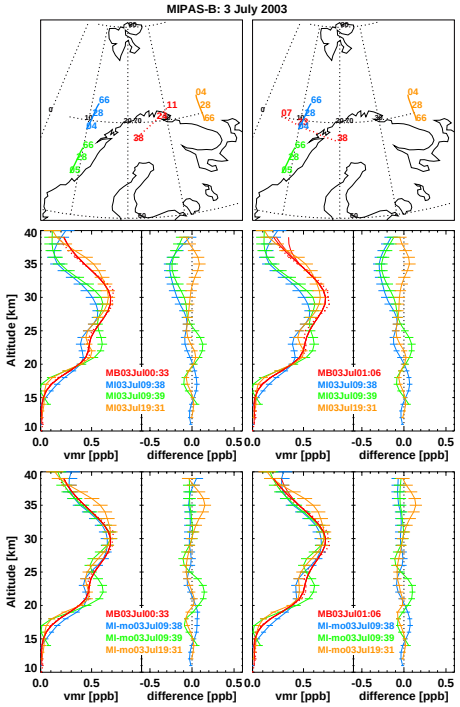

Fig. 4. Top and middle panel: same as Fig. 2 but for the validation campaign on 2/3 July 2003. The bottom panels show the CTM transformed (see Eq. 2) MIPAS vmr profiles $\boldsymbol{x}_{\mathrm{MIPAS}}^{\mathrm{trans}}$ (labelled MI-mo in the legend) in their right parts and the related difference profiles $\boldsymbol{x}_{\mathrm{MIPAS}}^{\mathrm{trans}} - \tilde{\boldsymbol{x}}_{\mathrm{ref}}$ in their left parts.

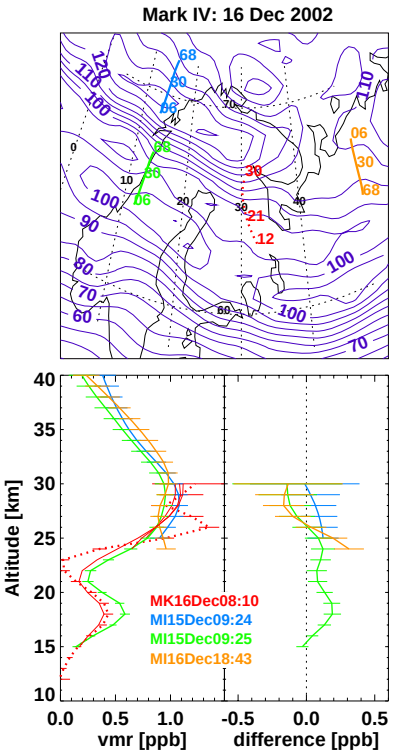

Fig. 5. Same as Fig. 2 but for the Mark IV flight on 16 December 2002. Blue contour lines in the maps show the fields of potential vorticity (PV) (units: $\mathrm{K\,m^2\,kg^{-1}\,s^{-1}}$) at 550 K potential temperature. Using the criterion by Nash et al. (1996) the vortex boundary is located at $86\,\mathrm{K\,m^2\,kg^{-1}\,s^{-1}}$.

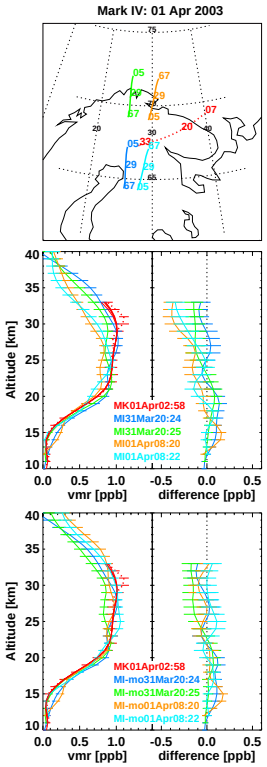

Fig. 6. Top and middle panels: same as Fig. 2 but for the Mark IV flight on 1 April 2003. The bottom panel shows the CTM transformed (see Eq. 2) MIPAS vmr profiles $\boldsymbol{x}_{\mathrm{MIPAS}}^{\mathrm{trans}}$ in the right part (labelled MI-mo in the legend) and the related difference profiles $\boldsymbol{x}_{\mathrm{MIPAS}}^{\mathrm{trans}} - \tilde{\boldsymbol{x}}_{\mathrm{ref}}$ in the left part.

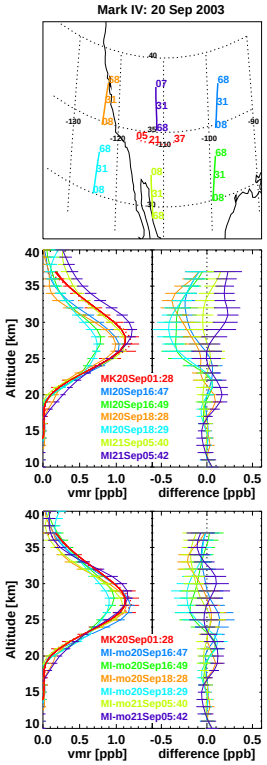

Fig. 7. Top and middle panels: same as Fig. 2 but for the Mark IV flight on 20 September 2003. The bottom panel shows the CTM transformed (see Eq. 2) MIPAS vmr profiles $\boldsymbol{x}_{\mathrm{MIPAS}}^{\mathrm{trans}}$ in the left part (labelled MI-mo in the legend) and the related difference profiles $\boldsymbol{x}_{\mathrm{MIPAS}}^{\mathrm{trans}} - \tilde{\boldsymbol{x}}_{\mathrm{ref}}$ in the right part.

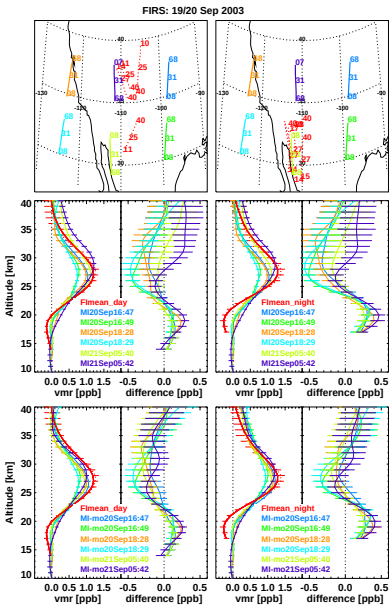

Fig. 8. Top left: location of FIRS2 daytime (red) and all MIPAS (other colours) limb scans for the balloon flight on 19/20 September 2003. Top right: location of FIRS2 nighttime (red) and all MIPAS (other colours) scans. Numbers indicate the positions of selected tangent points. Middle left column: Mean daytime altitude profiles of $ClONO_2$ from FIRS2 (dotted, red, $\boldsymbol{x}_{\mathrm{ref}}$ in Eq. 1) and MIPAS (solid, other colours, $\boldsymbol{x}_{\mathrm{MIPAS}}$). Middle right column: Same as the left column but for the nighttime mean FIRS2 profile. Bars indicate estimated total random errors. Bottom panels right part: Difference profiles $\boldsymbol{x}_{\mathrm{MIPAS}} - \tilde{\boldsymbol{x}}_{\mathrm{ref}}$ and combined errors for each MIPAS scan. The bottom panel shows the CTM transformed (see Eq. 2) MIPAS vmr profiles $\boldsymbol{x}_{\mathrm{MIPAS}}^{\mathrm{trans}}$ in the left part (labelled MI-mo in the legend) and the related difference profiles $\boldsymbol{x}_{\mathrm{MIPAS}}^{\mathrm{trans}} - \tilde{\boldsymbol{x}}_{\mathrm{ref}}$ in the right part.

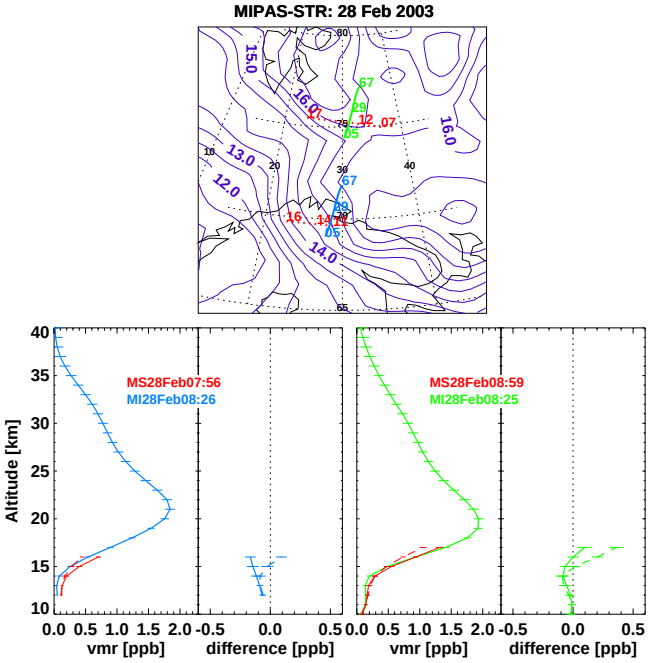

Fig. 9. Top: location of MIPAS-STR (red) and coincident MIPAS (other colours) limb scans during the Geophysica Envisat validation campaign on 28 February 2003. Below: MIPAS-STR $ClONO_2$ profiles retrieved with standard (red solid) and with MIPAS results (red dashed) as a-priori profiles in comparison with $ClONO_2$ from MIPAS.

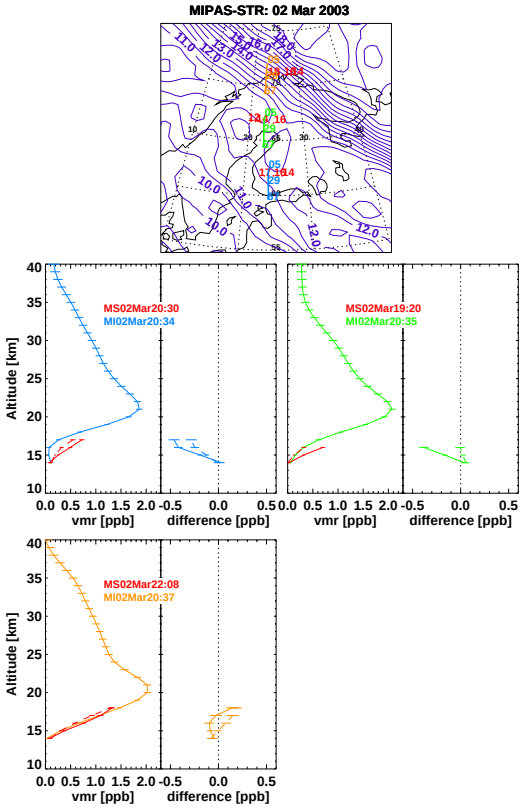

Fig. 10. Same as in Fig. 9 but for 2 March 2003.

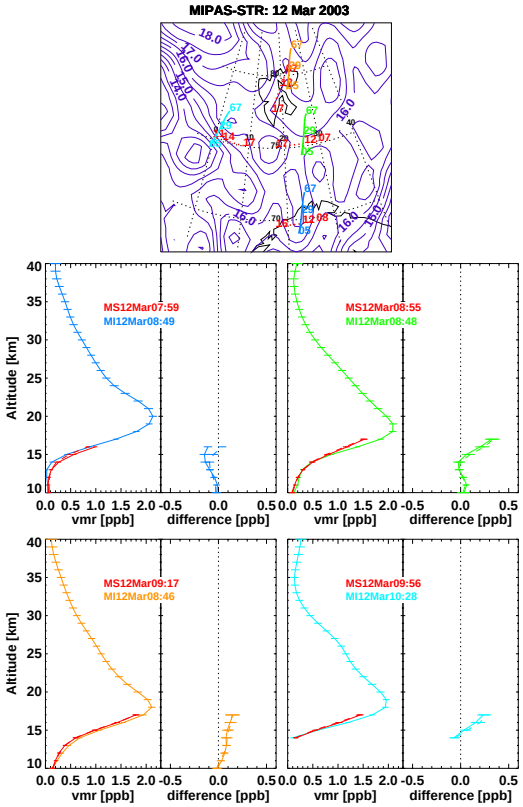

Fig. 11. Same as in Fig. 9 but for 12 March 2003.

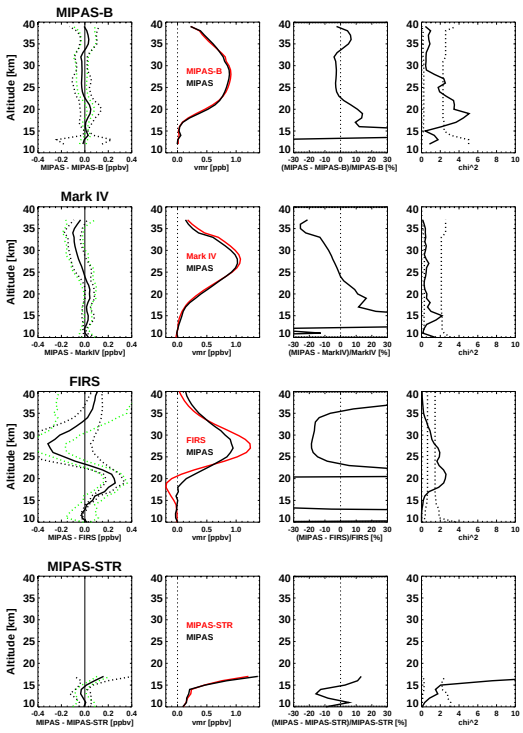

Fig. 12. Summary of MIPAS-B, Mark IV, FIRS and MIPAS-STR comparisons with MIPAS. First column: mean difference profiles $\bar{\boldsymbol{\delta}}$ (black solid), 95% confidence interval ($\pm 2\boldsymbol{\sigma}_{\bar{\delta},\mathrm{std}}$) (black dotted), and estimated total errors $\pm 2\boldsymbol{\sigma}_{\bar{\delta},\mathrm{err}}$ (green dotted) of the mean difference profiles. Second column: mean profiles. Third column: relative difference profiles. Fourth column: χ^2 profile (black solid) and 95% confidence interval for χ^2 (black dotted).

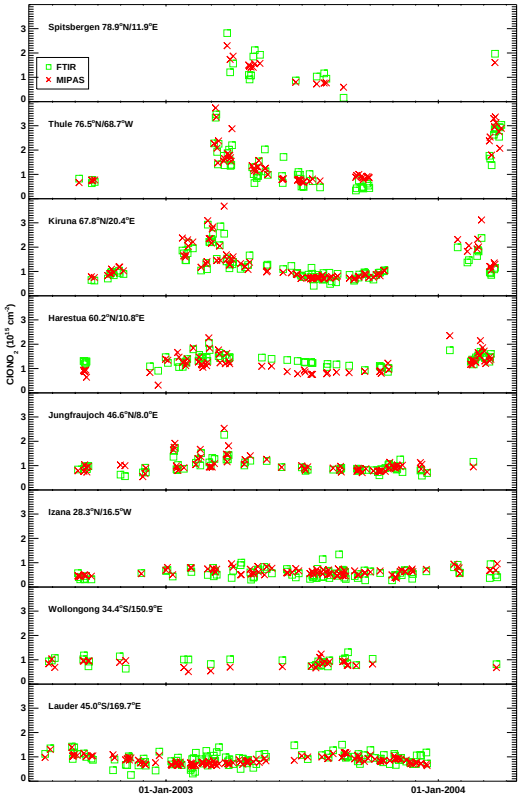

Fig. 13. Comparison between MIPAS (red) and FTIR (green) daily mean column amounts versus time for the collocation criterion $\Delta d_{\max}$=800 km, $\Delta t_{\max}$=8 h, and $\Delta pv_{\max}$=3×10^{-6} Km^2 kg^{-1} s^{-1} at 475 K.

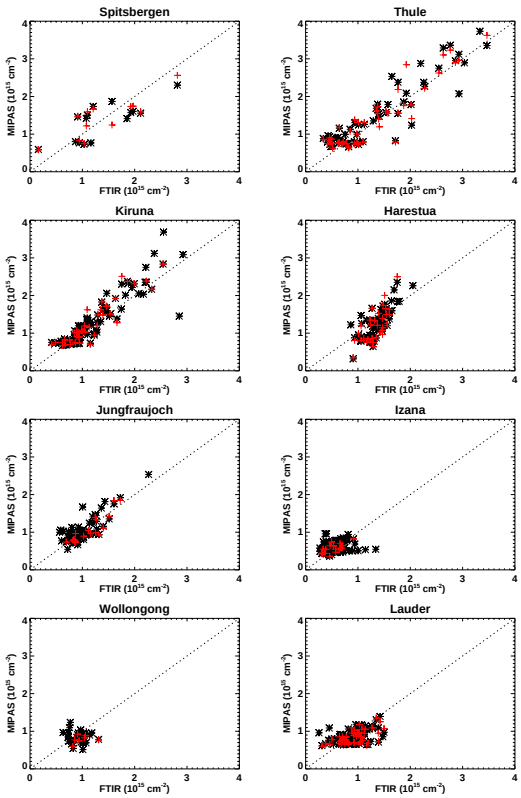

Fig. 14. Scatterplots between MIPAS and FTIR daily mean column amounts for the collocation criterion $\Delta d_{\max}$=800 km, $\Delta t_{\max}$=8 h, and $\Delta pv_{\max}$=3×10^{-6} Km^2 kg^{-1} s^{-1} at 475 K (black stars) and $\Delta d_{\max}$=400 km, $\Delta t_{\max}$=4 h, and $\Delta pv_{\max}$=3×10^{-6} Km^2 kg^{-1} s^{-1} at 475 K (red crosses).

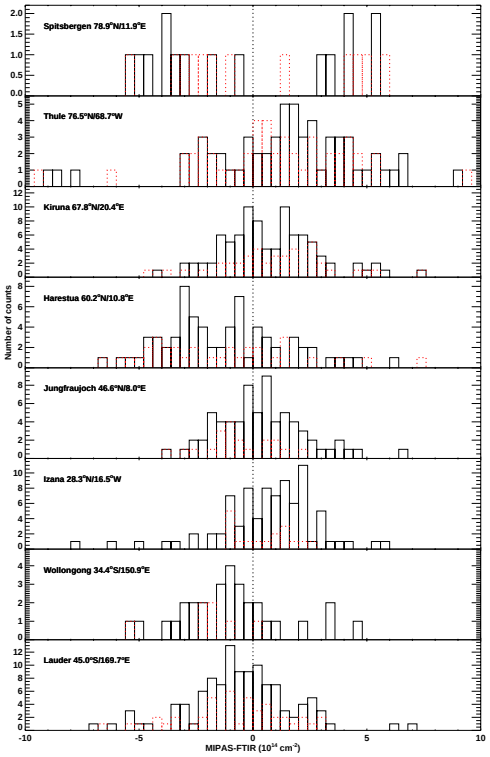

Fig. 15. Histograms of the column amounts daily differences for the collocation criterion $\Delta d_{\max}$=800 km, $\Delta t_{\max}$=8 h, and $\Delta pv_{\max}$=3 × 10^{-6} $\mathrm{Km^2\,kg^{-1}\,s^{-1}}$ at 475 K (black solid) and $\Delta d_{\max}$=400 km, $\Delta t_{\max}$=4 h, and $\Delta pv_{\max}$=3×10^{-6} $\mathrm{Km^2\,kg^{-1}\,s^{-1}}$ at 475 K (red dotted).

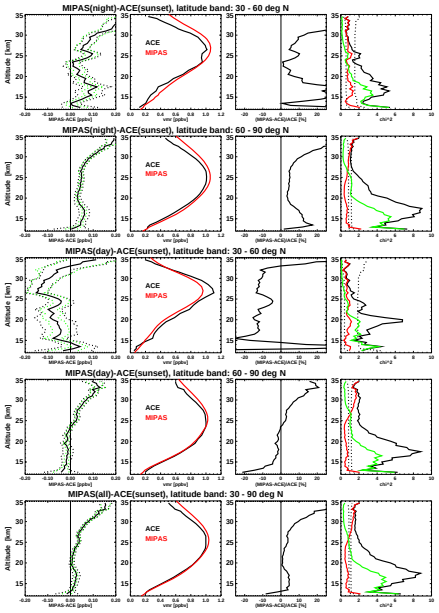

Fig. 16. Comparison between MIPAS and ACE-FTS vertical profiles of $ClONO_2$ in February and March 2003. The top two rows show MIPAS nighttime observations for the latitude bands 30–60° N and 60–90° N. Rows three and four contain MIPAS daytime measurements and the bottom row is the result for all co-incidences. First column: mean difference profiles $\bar{\boldsymbol{\delta}}$ (black solid), 95% confidence interval ($\pm 2\boldsymbol{\sigma}_{\bar{\delta},\mathrm{std}}$) (black dotted), and and estimated errors $\pm 2\boldsymbol{\sigma}_{\bar{\delta},\mathrm{err}}$ (green dotted) of the mean difference profiles. Second column: mean profiles. Third column: relative difference profiles. Fourth column: χ^2 profile (blacks solid) and 95% confidence interval for χ^2 (black dotted), coloured solid curves include coincidence errors derived on basis of MIPAS observations (red) and KASIMA CTM (green).

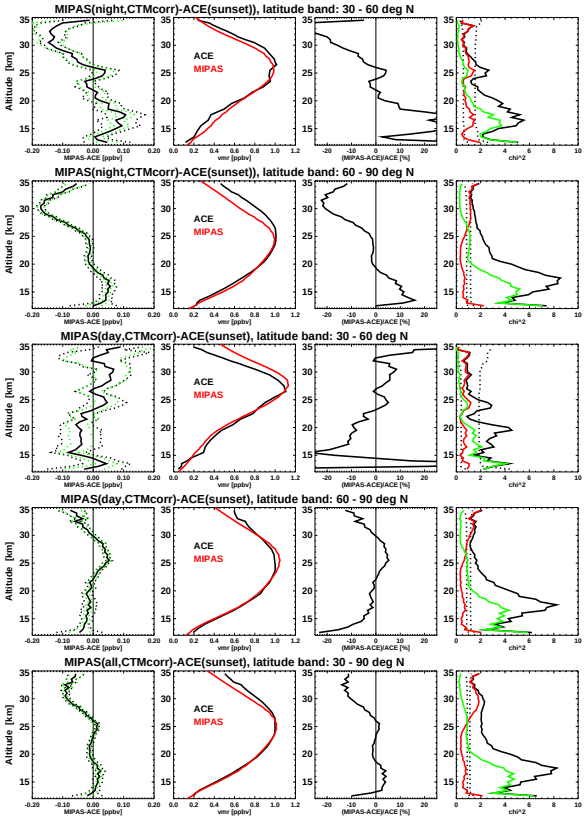

Fig. 17. Same as Fig. 16 but with a KASIMA CTM model correction of the MIPAS results.